

## CHAPTER 1

### NORMCONSERVING PSEUDOPOTENTIALS FOR THE EXACT EXCHANGE FUNCTIONAL

E. Engel, A. Höck, R. N. Schmid and R. M. Dreizler,  
*Institut für Theoretische Physik, Universität Frankfurt, D-60054  
 Frankfurt/Main, Germany  
 E-mail: engel@math.uni-frankfurt.de*

We dedicate this paper to Prof. Robert G. Parr on the occasion of his 80<sup>th</sup> birthday. The contributions of Bob Parr to the development and application of density functional theory have been a source of constant inspiration to the early adherents as well as to the late followers of this branch of many-body theory.

#### Contents

|  |    |
|--|----|
| 1. Introduction  | 2  |
| 2. Construction of Normconserving Pseudopotentials       | 7  |
| 3. Results Obtained with the LDA                         | 12 |
| 3.1. Atoms   | 12 |
| 3.2. Diatomic Molecules                                  | 13 |
| 3.3. Solids  | 15 |
| 4. Results Obtained with the Exact Exchange              | 16 |
| 4.1. Atoms   | 17 |
| 4.2. Diatomic Molecules                                  | 18 |
| 4.3. Detailed Analysis of OPM Pseudopotentials: Al       | 20 |
| 4.4. <i>A Posteriori</i> Damping of Long-Range Structure | 27 |
| 5. Selfconsistent Normconserving Pseudopotentials        | 33 |
| 6. Concluding Remarks                                    | 37 |
| Acknowledgements   | 38 |
| Appendix A. Technical Details                            | 38 |
| Appendix B. Multipole Expansion of OPM Pseudopotential   | 40 |
| References   | 41 |

## 1. Introduction

Pseudopotential (PP) calculations within the framework of density functional theory (DFT)<sup>1</sup> have become a standard tool for the study of complex many-electron systems. The PP approach greatly enhances the efficiency of electronic structure calculations by eliminating the more or less inert core electrons from the poly-atomic selfconsistency problem. When combined with the local density approximation (LDA) for the exchange-correlation (xc) energy functional  $E_{xc}$  of DFT, plane-wave basis sets and the molecular dynamics technique,<sup>2,3</sup> an enormous spectrum of problems can be addressed (see e.g. Refs. 4-9).

Phillips and Kleinman,<sup>10</sup> building on the orthogonalized plane-wave method of Herring,<sup>11</sup> were the first to introduce the concept of an ionic PP experienced by the valence electrons. The PP emerged from requiring orthogonality between the frozen atomic core states and the bulk valence states. In order to achieve this aim the overlap between core and valence states is explicitly projected out from the basis set representation of the valence states (e.g. in terms of plane waves). After insertion of this representation into the selfconsistent equations for the valence states the overlap terms take the form of a nonlocal potential operator, which can be decomposed into a sum over the various angular momenta  $l$  of the atomic levels,<sup>10</sup>

$$\langle \mathbf{r} | \hat{v}_{ps} | \mathbf{r}' \rangle = \sum_{l=0}^{l_{\max}} \bar{v}_{ps,l}(r, r') \sum_{m=-l}^l Y_{lm}(\Omega) Y_{lm}^*(\Omega'). \quad (1)$$

The form (1) is particularly useful if a suitable local approximation can be found for the potential  $\bar{v}_{ps,l}(r, r')$ ,

$$\langle \mathbf{r} | \hat{v}_{ps} | \mathbf{r}' \rangle = \frac{\delta(r - r')}{r^2} \sum_{l=0}^{l_{\max}} v_{ps,l}(r) \sum_{m=-l}^l Y_{lm}(\Omega) Y_{lm}^*(\Omega'). \quad (2)$$

Phillips and Kleinman obtained this form by an approximate evaluation of the overlap integrals between the atomic core and the molecular or bulk valence states,<sup>10</sup> exploiting the strong localization of the core states. As an alternative Abarenkov and Heine<sup>12</sup> suggested constructing  $v_{ps,l}(r)$  in such a way that the experimental energy levels of the relevant atomic valence states would be reproduced by the single-particle levels corresponding to

$v_{\text{ps},l}(r)$ . They proposed a simple two parameter form for  $v_{\text{ps},l}(r)$ ,<sup>12</sup>

$$v_{\text{ps},l}^{\text{AH}}(r) = \begin{cases} A_l & \text{for } r \leq r_c \\ -Z_{\text{ion}}/r & \text{for } r \geq r_c \end{cases}. \quad (3)$$

where  $Z_{\text{ion}}$  denotes the charge of the ionic core. The two parameters, the depth of the potential in the core region,  $A_l$ , and the cutoff radius  $r_c$ , are then optimized so that the eigenvalues resulting from  $v_{\text{ps},l}^{\text{AH}}$  (in the relevant energy range) are as close as possible to the experimental spectrum, with the restriction that the lowest pseudostate is nodeless.

PP calculations would be further simplified if a single radial PP  $v_{\text{loc}}(r)$  was sufficient for all valence levels. This is the idea behind the Ashcroft empty-core potential<sup>13</sup> in which all  $A_l$  are set to zero,

$$v_{\text{ps}}^{\text{A}}(r) = \begin{cases} 0 & \text{for } r \leq r_c \\ -Z_{\text{ion}}/r & \text{for } r \geq r_c \end{cases}. \quad (4)$$

The applicability of completely local PPs, however, seems to be restricted to metals with their essentially undirected bonding (for a recent study see<sup>14</sup>).

The standard form of normconserving PPs<sup>15</sup> therefore preserves the semilocal structure of (2), but extracts a local component  $v_{\text{loc}}$  from the individual  $v_{\text{ps},l}$ . In this way, effectively, PPs are included for all higher angular momenta,

$$\begin{aligned} \langle \mathbf{r} | \hat{v}_{\text{ps}} | \mathbf{r}' \rangle &= v_{\text{loc}}(r) \delta^{(3)}(\mathbf{r} - \mathbf{r}') + \frac{\delta(r - r')}{r^2} \\ &\times \sum_{l=0}^{l_{\text{max}}} \left[ v_{\text{ps},l}(r) - v_{\text{loc}}(r) \right] \sum_{m=-l}^l Y_{lm}(\Omega) Y_{lm}^*(\Omega'). \end{aligned} \quad (5)$$

An important feature of (5) is the short range of the remaining semilocal part of the potential. The main advantage of normconserving PPs over the Abarenkov-Heine form, however, is the refined construction of  $v_{\text{ps},l}(r)$ . Relying on all-electron (AE), rather than on experimental information, the  $v_{\text{ps},l}$  are chosen so that the resulting atomic pseudo valence states exactly reproduce the corresponding AE valence states beyond the cutoff radius (which is now  $l$ -dependent,  $r_{c,l}$ ). As one wants the  $v_{\text{ps},l}$  to be local with respect to  $r$  this requires the AE reference calculation to be based on DFT with its multiplicative total potential.<sup>1</sup>

Given the AE information, the construction of  $v_{\text{ps},l}$  proceeds in two steps. In the first step a screened radial PP  $v_{\text{ps},l}^{\text{sc}}$  is generated:  $v_{\text{ps},l}^{\text{sc}}$  is the

total single-particle potential which has the desired pseudo valence state as lowest eigenstate. The identity of the pseudo with the AE state in the valence regime  $r \geq r_{c,l}$  requires  $v_{ps,l}^{sc}$  to be identical with the total AE Kohn-Sham potential, so that only the form of the PP in the core region has to be considered. For the extension of the PP into the core region different schemes have been suggested,<sup>15–19</sup> among which the Troullier-Martins (TM) approach<sup>19</sup> seems to be the most widely used. Compared with the original concept of Hamann, Schlüter and collaborators<sup>15</sup> the TM scheme produces somewhat smoother PPs and thus allows a restriction to smaller plane-wave basis sets in PP applications.

In a second step the interaction among the valence electrons (and their self-interaction) is eliminated from  $v_{ps,l}^{sc}$  by the so-called unscreening procedure. This is required as PPs are usually applied to molecules or solids within a self-consistent framework, typically nonrelativistic spin-density functional theory. The simplest approach is linear unscreening,

$$v_{ps,l}(r) = v_{ps,l}^{sc}(r) - v_H([n_{v,ps}]; r) - v_{xc}([n_{v,ps}]; r), \quad (6)$$

where  $v_H[n_{v,ps}]$  denotes the electrostatic (Hartree) interaction among the valence electrons with pseudo valence density  $n_{v,ps}$ ,

$$v_H([n]; r) = e^2 \int d^3r' \frac{n(r')}{|\mathbf{r} - \mathbf{r}'|}, \quad (7)$$

and  $v_{xc}[n_{v,ps}]$  is their exchange-correlation (xc) interaction,

$$v_{xc}([n]; r) = \frac{\delta E_{xc}[n]}{\delta n(\mathbf{r})}. \quad (8)$$

The xc-energy functional  $E_{xc}[n]$  of DFT, however, is a nonlinear functional of the density  $n$ . The unscreening (6) thus implies a linearization of  $E_{xc}$  as far as the core-valence interaction is concerned. The actual nonlinearity of  $E_{xc}$  is often taken into account via nonlinear core corrections (nlccs),<sup>20</sup>

$$v_{ps,l}^{nlcc}(r) = v_{ps,l}^{sc}(r) - v_H([n_{v,ps}]; r) - v_{xc}([n_{v,ps} + n_c]; r). \quad (9)$$

i.e. by inclusion of the core density  $n_c$  in the nonlinear part of the unscreening potential. This procedure is particularly important for transition metal elements<sup>21,22</sup> for which the valence states have substantial overlap with semicore states. However, the nonlinearity of  $E_{xc}$  has to be taken into account even for first row elements (see e.g. Ref. 23 and Sec. 3 below).

Although the PP approach is mostly combined with the LDA for  $E_{xc}$ , it can equally well be used<sup>24,22</sup> together with semilocal xc-functionals such as the generalized gradient approximation (GGA).<sup>25,26</sup> First PP calculations based on orbital-dependent representations of  $E_{xc}$  have also been presented<sup>27-30</sup> in recent years. In these implicit density functionals<sup>31-39</sup> (for an overview see<sup>40</sup>) the Kohn-Sham (KS) orbitals  $\phi_k$  are used to characterize  $E_{xc}$ , rather than just the density  $n$ . The basic functional of this type is the exact exchange  $E_x$  of DFT,

$$E_x = -\frac{e^2}{2} \sum_{\epsilon_i, \epsilon_j \leq \epsilon_F} \int d^3r_1 \int d^3r_2 \frac{\phi_i^\dagger(\mathbf{r}_1)\phi_j(\mathbf{r}_1)\phi_j^\dagger(\mathbf{r}_2)\phi_i(\mathbf{r}_2)}{|\mathbf{r}_1 - \mathbf{r}_2|}, \quad (10)$$

where  $\epsilon_F$  is the Fermi energy. While an appropriate approximation for the correlation component of  $E_{xc}$  is still under debate,<sup>33-39</sup> the results from implicit functionals available so far already indicate the potential of this method.<sup>27,28,30,35,36,40-48</sup> Orbital-dependent functionals have, however, one major disadvantage compared with the LDA or GGA: The corresponding xc-potential has to be evaluated in an indirect fashion via the Optimized Potential Method (OPM),<sup>49,50</sup> which is computationally more involved than the calculation of LDA or GGA potentials. Consequently, the PP approach appears to be particularly attractive for this third generation of density functionals.

It has been noticed very early<sup>27</sup> that the use of the exact  $E_x$  for the construction of normconserving PPs leads to a technical problem. The first step of the PP construction, the generation of the screened PP, can proceed as for the LDA, with the total AE OPM potential serving as screened PP in the valence regime. The second step, the elimination of the interaction among the valence electrons from the screened PP, is no longer as simple. An important prerequisite for the success of normconserving PPs is the complete cancellation of the xc-component in the screened PP by  $v_{xc}[n_{v,ps}]$  in the large- $r$  regime. Otherwise the unscreened PP, i.e. the net potential representing the ionic core, does not exhibit a clean  $-Z_{ion}e^2/r$ -behavior far outside the core region. This cancellation is guaranteed for all (semi)local functionals like the LDA or GGA: As soon as the density of the core electrons vanishes, the resulting  $v_{xc}$  is completely determined by the local value of the valence density, both in the AE xc-potential (and thus the screened PP) and in  $v_{xc}[n_{v,ps}]$ . The situation is more complicated for fully nonlocal functionals as the exact exchange. Here the density in the

core regime affects the exchange potential in the valence regime, so that  $v_{xc}[n_{v,ps}]$  can differ from the AE exchange potential even for very large  $r$ . The resulting non-electrostatic long-range tail in the unscreened PP then acts as an additional repulsive or attractive force on neighbouring ions in poly-atomic situations. As a consequence, structural optimizations on the basis of such PPs can be seriously in error.

One way to resolve this problem is to resort to a fundamentally different PP construction scheme. For instance, the concept of energy-adjusted PPs,<sup>51</sup> used for the generation of Hartree-Fock-based PPs, guarantees the correct asymptotic behavior from the very outset. On the other hand, one can try to handle the problem within the framework of normconserving PPs, relying on a suitable modification of the PP construction scheme. The simplest modification is the *a posteriori* damping of the undesired structure,<sup>27</sup> which, however, introduces additional parameters and thus a certain arbitrariness of the final molecular or bulk results. As an alternative it has been suggested<sup>30</sup> to utilize normconserving LDA-PPs in molecular PP calculations with the exact exchange. The use of different xc-functionals for the PP construction and the poly-atomic calculation can, however, lead to significant errors.<sup>22</sup>

In this contribution we review the properties of the normconserving PPs obtained for the exact  $E_x$  via the OPM (subsequently denoted by OPM-PP). We start with a summary of the construction of OPM-PPs within the relativistic version<sup>52</sup> of the TM scheme<sup>19</sup> (in Sec. 2). In Sec. 3 we present some prototype results obtained with normconserving LDA-PPs, in order to provide a comparative background for the subsequent discussion of OPM-PPs. The properties of OPM-PPs are studied for atoms, molecules and solids in Sec. 4. For atoms we discuss  $s - p$  transfer energies of the second row elements as an example of atomic excitation energies as well as the energy gain resulting from the transition from a spherical to a nonspherical ground state density (Sec. 4.1). Both quantities probe the importance of the core-valence interaction. It turns out that, in the case of the exact exchange, the PPs reproduce the corresponding AE data better than their LDA counterparts. This indicates that, overall, the core-valence interaction is less relevant in the case of the exact exchange (in spite of the fact that it causes a spurious tail). The unmodified OPM-PPs are also applied to a set of 15 first and second row diatomic molecules (Sec. 4.2 — the technical details are given in Appendix A). A comparison of the spectroscopic con-

stants found with the OPM-PPs with the corresponding AE OPM values<sup>48</sup> demonstrates that the spurious long-range tail has only a limited effect on the bond lengths of diatomic molecules, but clearly affects their dissociation energies. The erroneous tail becomes more and more important with increasing number of neighbouring atoms in a poly-atomic system, as is shown by a calculation for bulk Aluminum.

A detailed analysis verifies explicitly that the long-range structure originates from the core-valence interaction, so that it cannot be eliminated by further optimization of the pseudo valence orbitals (Sec. 4.3). In view of this origin a nonlinear unscreening scheme analogous to the nlcc concept would constitute the most systematic way to eliminate the long-range structure (as shown in Sec. 4.3). However, the inclusion of core states in the evaluation of the molecular or bulk exchange potential substantially reduces the numerical efficiency of PP calculations. Given the limited importance of the core-valence interaction in the case of the exact exchange, it thus seems that some form of linear unscreening is mandatory.

We therefore examine the *a posteriori* damping of the long-range tail (Sec. 4.4). On the average, the damped PPs clearly yield improved molecular and bulk data compared with the unmodified PPs. However, variation of the damping parameters leads to a spread of the poly-atomic results which is not much smaller than the deviation of the unmodified PP values from the AE data. In order to resolve this ambiguity, we finally consider a novel PP construction scheme which eliminates the spurious tail in a parameter-free fashion<sup>53</sup> (Sec. 5). In this scheme an iterative procedure formulated within the framework of normconserving PPs eliminates the tail. The performance of the resulting selfconsistent normconserving PPs in molecular and bulk calculations is superior to that of linearly unscreened LDA-PPs. This demonstrates the basic compatibility of the OPM with the concept of normconserving PPs.

## 2. Construction of Normconserving Pseudopotentials

In this Section we summarize the construction of normconserving PPs. In the first step a screened PP  $v_{ps,l}$  must be derived from AE results for the atom of interest. In order to cover the complete periodic table one relies on a relativistic AE treatment.<sup>15</sup> This leads to  $j$ -dependent PP components  $v_{ps,lj}$  in accordance with the  $j$ -dependence of the individual valence states. However, while the core states directly experience the relativistic effects,

the pseudo valence states and potentials are in most cases only indirectly affected via the orthogonality requirement (for a discussion of the relativistic corrections to PPs see Ref. 52). The  $j$ -independent components of the PP (5) required for the usual nonrelativistic PP calculations for molecules or solids are obtained from a  $j$ -average over the  $v_{\text{ps},lj}$ ,<sup>15</sup>

$$v_{\text{ps},l}(r) = \sum_{j=l\pm 1/2} \frac{2j+1}{4l+2} v_{\text{ps},lj}(r). \quad (11)$$

Although we only deal with first and second row atoms, we shall discuss the PP construction within the relativistic approach (11). For the construction of the nonrelativistic PPs, which are consistently used in all comparisons with nonrelativistic AE data, we apply the relativistic scheme in the limit  $c \rightarrow \infty$ <sup>a</sup>.

For the construction of the individual  $v_{\text{ps},lj}$  we use the relativistic form<sup>52</sup> of the Troullier-Martins (RTM) scheme.<sup>19</sup> The RTM scheme starts with a relativistic AE calculation, which requires the solution of the radial KS equations of relativistic DFT (for details and notation see Ref. 36),

$$c \left( \partial_r + \frac{\kappa}{r} \right) a_{nlj}(r) = \left( 2mc^2 - v_{\text{s}}(r) + \epsilon_{nlj} \right) b_{nlj}(r) \quad (12)$$

$$c \left( \partial_r - \frac{\kappa}{r} \right) b_{nlj}(r) = \left( v_{\text{s}}(r) - \epsilon_{nlj} \right) a_{nlj}(r), \quad (13)$$

where

$$v_{\text{s}}(r) = -\frac{Ze^2}{r} + v_{\text{H}}(r) + v_{\text{xc}}(r) \quad (14)$$

$$v_{\text{H}}(r) = 4\pi e^2 \left\{ \frac{1}{r} \int_0^r x^2 dx n(x) + \int_r^\infty x dx n(x) \right\} \quad (15)$$

$$n(r) = \sum_{nlj} \Theta_{nlj} \frac{a_{nlj}(r)^2 + b_{nlj}(r)^2}{4\pi r^2}, \quad (16)$$

<sup>a</sup>In the case of orbital-dependent xc-functionals this limiting procedure does not always yield exactly the same PPs as an inherently nonrelativistic approach. For open valence shells with  $l \neq 0$  differences originate from the average over all available  $m$ -substates which is required to obtain a spherical AE potential and density (see e.g.<sup>36</sup>): In the relativistic case the  $m$ -average only extends over the  $2j+1$  substates with given  $j$ , while it includes all  $4l+2$  substates in the nonrelativistic situation. However, the final PPs differ only marginally.

and  $\Theta_{nlj}$  denotes the occupation of each  $nlj$ -subshell ( $\kappa = -2(j-l)(j+1/2)$  — We use the standard form of the spherical spinors as given by Rose<sup>54</sup>). For explicitly density-dependent functionals the functional derivative (8) can be taken analytically. In the case of the exact exchange it has to be evaluated numerically via the relativistic extension<sup>36</sup> of the OPM.<sup>49,50</sup> For spherical systems the relativistic OPM for the exact exchange requires the solution of ( $T$  denotes the transpose)

$$\int_0^\infty dr' K(r, r') v_x(r') = Q_x(r) \quad (17)$$

$$K(r, r') = \sum_{nlj} \Theta_{nlj} \varphi_{nlj}^T(r) G_{nlj}(r, r') \varphi_{nlj}(r') \quad (18)$$

$$Q_x(r) = \frac{1}{2} \sum_{nlj} \int_0^\infty dr' \varphi_{nlj}^T(r) G_{nlj}(r, r') \frac{\delta E_x}{\delta \varphi_{nlj}^T(r')} \quad (19)$$

$$E_x = -\frac{e^2}{2} \sum_{nlj, n'l'j'} \sum_{L=0}^\infty \Theta_{nlj} \Theta_{n'l'j'} C_{nlj, n'l'j', L} \times \int_0^\infty dr \int_0^\infty dr' \frac{r^L}{r^{L+1}} \varphi_{n'l'j'}^T(r) \varphi_{nlj}(r) \varphi_{n'l'j'}^T(r') \varphi_{nlj}(r') \quad (20)$$

$$G_{nlj}(r, r') = \Gamma_{nlj}(r, r') + C_{nlj} \varphi_{nlj}(r) \varphi_{nlj}^T(r') - \int_0^\infty dr'' \Gamma_{nlj}(r, r'') \varphi_{nlj}(r'') \varphi_{nlj}^T(r') - \int_0^\infty dr'' \varphi_{nlj}(r) \varphi_{nlj}^T(r'') \Gamma_{nlj}(r'', r') \quad (21)$$

$$C_{nlj} = \int_0^\infty dr \int_0^\infty dr' \varphi_{nlj}^T(r) \Gamma_{nlj}(r, r') \varphi_{nlj}(r') \quad (22)$$

$$\Gamma_{nlj}(r, r') = \Theta(r - r') \varphi_{nlj}(r) \chi_{nlj}^T(r') + \Theta(r' - r) \chi_{nlj}(r) \varphi_{nlj}^T(r'). \quad (23)$$

Here  $\varphi_{nlj}$  denotes the (real) radial spinor,

$$\varphi_{nlj}(r) = \begin{pmatrix} a_{nlj}(r) \\ b_{nlj}(r) \end{pmatrix}, \quad (24)$$

and  $\chi_{nlj}$  is the nonnormalizable solution of the radial KS equations (12), (13) for the eigenvalue  $\epsilon_{nlj}$  (for the definition of the angular momentum coupling coefficients  $C_{nlj, n'l'j', L}$  see Appendix A.1 of Ref. 36). In the case

of open subshells Eq. (20) implies a spherical average, which is equivalent to averaging over all available  $m$ -substates.

Given the atomic AE OPM solutions, i.e. the large and small components of the radial AE orbitals (AEOs),  $a_{nlj}$ ,  $b_{nlj}$ , the corresponding eigenvalues  $\epsilon_{nlj}$  and the total AE potential  $v_s$ , the construction of screened PP  $v_{\text{ps},lj}^{\text{sc}}$  for the case of the exact  $E_x$  proceeds as for the LDA. The large component of the pseudoorbital (PO),  $a_{\text{ps},lj}$ , is obtained from its AE counterpart by the ansatz

$$a_{\text{ps},lj}(r) = \begin{cases} a_{nlj}(r) & \text{for } r > r_{c,l} \\ r^{l+1} \exp[p(r)] & \text{for } r \leq r_{c,l} \end{cases} \quad (25)$$

$$p(r) = \sum_{i=0}^6 c_{2i} r^{2i}. \quad (26)$$

The associated screened PP reads<sup>52</sup>

$$v_{\text{ps},lj}^{\text{sc}} = \begin{cases} v_s & \text{for } r > r_{c,l} \\ v_{\text{ps},lj}^{\text{sc,nr}} + \delta v_{lj} & \text{for } r \leq r_{c,l} \end{cases} \quad (27)$$

$$v_{\text{ps},lj}^{\text{sc,nr}} = \epsilon_{nlj} + \frac{l+1}{r} \frac{p'}{m} + \frac{p'' + (p')^2}{2m} \quad (28)$$

$$\delta v_{lj} = \frac{(v_{\text{ps},lj}^{\text{sc,nr}} - \epsilon_{nlj})^2}{2mc^2} + \frac{(v_{\text{ps},lj}^{\text{sc,nr}})'}{4m^2 c^2} \left( \frac{a'_{\text{ps},lj}}{a_{\text{ps},lj}} + \frac{\kappa}{r} \right), \quad (29)$$

where the primes denote derivatives with respect to  $r$ . The corresponding small component  $b_{\text{ps},lj}$  of the PO then follows from the radial Dirac equation,

$$b_{\text{ps},lj}(r) = \begin{cases} b_{nlj}(r) & \text{for } r > r_c \\ \frac{c[(l+1+\kappa)/r + p'(r)]a_{\text{ps},lj}(r)}{2mc^2 - v_{\text{ps},lj}^{\text{sc}}(r) + \epsilon_{nlj}} & \text{for } r \leq r_c \end{cases}. \quad (30)$$

The coefficients  $c_{2i}$  are determined by requiring continuity of  $a_{\text{ps},lj}$  and its first four derivatives at the cutoff radius  $r_{c,l}$ , a smooth PP at the origin,  $(v_{\text{ps},lj}^{\text{sc,nr}})''(0) = 0$ , as well as proper normalization,

$$\int_0^{r_c} dr [a_{nlj}(r)^2 + b_{nlj}(r)^2] = \int_0^{r_c} dr [a_{\text{ps},lj}(r)^2 + b_{\text{ps},lj}(r)^2]. \quad (31)$$

Once the POs and screened PPs are evaluated it only remains to eliminate the interaction among the valence electrons from the screened PP. It is this unscreening procedure in which the difference between LDA and

OPM shows up. In the case of linear unscreening one has to evaluate both  $v_H$  and  $v_{xc}$  for the pseudo valence density

$$n_{v,ps}(r) = \sum_{\text{occ.val.orb.}} \Theta_{lj} \frac{a_{ps,lj}(r)^2 + b_{ps,lj}(r)^2}{4\pi r^2}. \quad (32)$$

In the case of the LDA the evaluation of  $v_{xc}([n_{v,ps}], r)$  reduces to the insertion of  $n_{v,ps}$  into the analytically given functional  $v_{xc}^{\text{LDA}}[n]$ . In the OPM, on the other hand, the functional derivative  $\delta E_{xc}/\delta n$  is essentially replaced by functional derivatives of  $E_{xc}$  with respect to the KS orbitals, using the unique correspondence between  $n$  and  $\phi_k$ . However, as the POs belong to different screened PPs for  $r < r_{c,l}$ ,  $n_{v,ps}$  does not uniquely determine the complete set of POs from a rigorous point of view. This questions the legitimacy of the transition from  $\delta/\delta n$  to  $\delta/\delta\phi_k$ .<sup>55</sup> On the other hand, in the physically relevant valence region all  $v_{ps,lj}^{\text{sc}}$  are identical with the AE potential, and the POs are identical with the corresponding AEOs. In addition, the basic concept of PPs implies that the form of the POs in the core region is not really important for their physical properties (as long as the POs are normconserving and smooth). In spite of the nonlocality of  $E_x$  the form of the POs for  $r < r_{c,l}$  thus plays only a limited role for  $v_x[n_{v,ps}]$  in the valence regime (see Fig. 1 of Ref. 29). This suggests utilizing the standard form of the OPM also for the calculation of  $v_x[n_{v,ps}]$ . In the case of the unscreening potential  $v_x[n_{v,ps}]$  the sums in Eqs. (18)–(20) then reduce to sums over the occupied valence orbitals and  $\varphi_{nlj}$  simply represents the POs,

$$\varphi_{nlj}(r) \longrightarrow \varphi_{ps,lj}(r) = \begin{pmatrix} a_{ps,lj}(r) \\ b_{ps,lj}(r) \end{pmatrix}.$$

The concept of nlccs can, in principle, also be applied in the framework of the OPM. In this case one would combine the valence POs with the AE core orbitals in Eqs. (18)–(20). In contrast to the LDA, however, the form of the POs in the core region is used in Eqs. (18)–(20), so that one would expect that the lack of orthogonality between AE core and pseudo valence orbitals becomes noticeable. In addition, the concept of nlccs can in practice only be used if a smooth truncation of  $n_c$  below some core-cutoff radius  $r_{nlcc}$  is possible, e.g. in the form

$$n_{c,ps}(r) = \begin{cases} n_0 + \sum_{i=3}^6 n_i r^i & \text{for } r < r_{nlcc} \\ n_c(r) & \text{for } r \geq r_{nlcc} \end{cases}. \quad (33)$$

Without this truncation the representation of  $n_c$  in terms of basis functions and/or integrations over  $n_c$  would become exceedingly difficult. Unfortunately, it is very unlikely that the OPM equations (17)–(23) allow an analogous manipulation of the core orbitals as this would massively affect the orthonormality of the orbitals. One can thus only hope that the inclusion of the outermost core shell in  $v_{xc}[n_{v,ps} + n_c]$  is sufficient. The question will be further investigated in Sec. 4.3.

### 3. Results Obtained with the LDA

In order to set the stage for an analysis of OPM-PPs we present some LDA<sup>56</sup> results. This illustrates the high level of accuracy that can be reached with normconserving PPs and provides the background for a judgement of the quality of OPM-PPs.

#### 3.1. Atoms

In Tab. 1 we list the  $3s - 3p$  transfer energies of second row atoms, comparing PP with AE results. All calculations are nonrelativistic and utilize spherically averaged densities. Wherever possible, two types of excitations are shown: In the first case, the minority spin ( $\downarrow$ )  $3s$ -electron is transferred to the majority spin ( $\uparrow$ )  $3p$ -orbital, so that the excited state has a larger spin-polarization (magnetic moment) than the ground state. In the second case, the  $3s_{\downarrow}$ -electron goes into the  $3p_{\downarrow}$ -state, leaving the magnetic moment unchanged. For the last transition even the PPs not including nlccs yield excitation energies which agree rather well with the AE data. They perform particularly well if the net spin-polarization is small, as for Mg, Al and Cl. On the other hand, for the transitions involving a spin-flip the AE data are substantially underestimated by the PPs without nlccs. The maximum error is found for Si, for which the excited state exhibits the highest possible spin-polarization. The stability of the high-spin excited state is clearly overestimated. Table 1 demonstrates that nlccs are required for an accurate description of states with high magnetic moments (compare<sup>23</sup>). Inclusion of the unpolarized core density in the xc-functional reduces the energy gain obtained by an increase of spin-polarization which leads to improved ground state and excited state energies.

Another atomic quantity of interest is the energy gain obtained for open-shell atoms when releasing the restriction of spherical symmetry for the

Table 1.  $s-p$  transfer energies  $\Delta E = E_{\text{tot}}(3s^1 3p^{n+1}) - E_{\text{tot}}(3s^2 3p^n)$  of second row atoms: PP versus AE results (all energies in eV).

|    | mode    | $3s_{\downarrow} \rightarrow 3p_{\uparrow}$ |      | $3s_{\downarrow} \rightarrow 3p_{\downarrow}$ |       |
|----|---------|---|------|---|-------|
|    |         | LDA   | OPM  | LDA   | OPM   |
| Mg | AE      | 2.80  | 1.84 | 3.44  | 3.12  |
|    | PP      | 2.69  | 1.79 | 3.40  | 3.10  |
|    | PP+nlcc | 2.80  |      | 3.44  |       |
| Al | AE      | 3.61  | 2.32 | 5.01  | 4.78  |
|    | PP      | 3.41  | 2.21 | 4.96  | 4.70  |
|    | PP+nlcc | 3.61  |      | 5.01  |       |
| Si | AE      | 4.31  | 2.47 | 6.57  | 6.38  |
|    | PP      | 3.98  | 2.29 | 6.48  | 6.25  |
|    | PP+nlcc | 4.29  |      | 6.57  |       |
| P  | AE      |   |      | 8.14  | 7.96  |
|    | PP      |   |      | 8.02  | 7.79  |
|    | PP+nlcc |   |      | 8.14  |       |
| S  | AE      |   |      | 9.95  | 11.36 |
|    | PP      |   |      | 9.89  | 11.22 |
|    | PP+nlcc |   |      | 9.95  |       |
| Cl | AE      |   |      | 11.79   | 15.21 |
|    | PP      |   |      | 11.76   | 15.12 |
|    | PP+nlcc |   |      | 11.78   |       |

density, in accord with their exact form.<sup>57</sup> This has also some very practical implications: The slightly lower atomic ground state energies calculated with nonspherical densities generally improve the resulting dissociation energies of molecules.<sup>58</sup> As in the case of the energy difference between states with different magnetic moments the energy gain from nonsphericity is indicative of the importance of the core-valence interaction. The presence of the essentially spherical core density stabilizes the spherical components in the valence density. This can be seen explicitly in Tab. 2, in which the relevant data for Oxygen are given. The AE-calculations lead to an energy gain of 0.11 eV, while the PP calculations on the basis of a linearly unscreened PP yields 0.17 eV. This difference disappears as soon as nlccs are included (compare<sup>23</sup>).

### 3.2. Diatomic Molecules

As a second example we consider molecular ground state properties. The spectroscopic constants obtained with the LDA for 15 first and second row diatomic molecules are listed in Tabs. 3 and 4 (see Appendix A for the

Table 2. Atomic ground state energy of Oxygen: Energy gain from non-spherical density. The calculations for the exact exchange are based on the KLI approximation (all calculations are strictly nonrelativistic).

| Mode    | $E_{xc}$ |     | state                    |                   | $-E_{tot}$<br>[Hartree] | $\Delta E_{tot}$<br>[eV] |
|---------|----------|-----|--------------------------|-------------------|-------------------------|--------------------------|
|         | x        | c   | spin $\uparrow$          | spin $\downarrow$ |                         |                          |
| AE      | LDA      | LDA | $2s2p^3$                 | $2s2p^1$          | 74.52741                |                          |
| AE      | LDA      | LDA | $2\sigma 1\pi^2 3\sigma$ | $2\sigma 3\sigma$ | 74.53135                | 0.107                    |
| PP      | LDA      | LDA | $2s2p^3$                 | $2s2p^1$          | 15.80944                |                          |
| PP      | LDA      | LDA | $2\sigma 1\pi^2 3\sigma$ | $2\sigma 3\sigma$ | 15.81557                | 0.167                    |
| PP+nlcc | LDA      | LDA | $2s2p^3$                 | $2s2p^1$          | 18.73802                |                          |
| PP+nlcc | LDA      | LDA | $2\sigma 1\pi^2 3\sigma$ | $2\sigma 3\sigma$ | 18.74203                | 0.109                    |
| AE      | exact    | —   | $2s2p^3$                 | $2s2p^1$          | 74.81167                |                          |
| AE      | exact    | —   | $2\sigma 1\pi^2 3\sigma$ | $2\sigma 3\sigma$ | 74.81680                | 0.140                    |
| PP      | exact    | —   | $2s2p^3$                 | $2s2p^1$          | 15.68921                |                          |
| PP      | exact    | —   | $2\sigma 1\pi^2 3\sigma$ | $2\sigma 3\sigma$ | 15.69425                | 0.137                    |

technical details of the two-center calculations). For all molecules the PP results obtained without and with nlccs are listed together with the AE data. In order to be consistent with the nonrelativistic AE data, all PPs have been constructed in a nonrelativistic fashion. For both sets of molecules the average absolute deviations of the PP results from the AE reference values are given as well.

Tables 3 and 4 document the well-known success of normconserving PPs. Even without nlccs the average error in the bond length ( $R_e$ ) is no larger than 0.03 Bohr. This deviation is reduced to less than 0.01 Bohr by inclusion of nlccs. Use of nlccs is particularly important for the dissociation energy ( $D_e$ ) (even for the first row – compare<sup>23</sup>): The average error of 0.24 eV found for the first row molecules without nlccs is not very satisfactory. This error mainly originates from molecules whose constituents are “strongly” spin-polarized, with Nitrogen being the prime example. For these systems  $D_e$  is generally underestimated without nlccs, as a consequence of an overestimation of the atomic ground state energies. This is consistent with the observation that quite generally the energy of high-spin states is overestimated by PPs without nlccs. As in the case of the  $s - p$  transfer energies the difficulties with high-spin states are resolved by inclusion of nlccs: The resulting average error of 0.05 eV for  $D_e$  defines the level of accuracy at which one also aims with OPM-PPs.

Table 3. Bond length  $R_e$ , dissociation energy  $D_e$  (including zero-point energy) and harmonic frequency  $\omega_e$  of first row diatomic molecules: PP versus AE LDA results.<sup>56,59</sup>

|                                   | mode    | $R_e$  | $D_e$  | $\omega_e$          |
|-----------------------------------|---------|--------|--------|---------------------|
|                                   |         | [Bohr] | [eV]   | [cm <sup>-1</sup> ] |
| Li <sub>2</sub><br><sup>1</sup> Σ | AE      | 5.118  | 1.030  | 338                 |
|                                   | PP      | 5.029  | 1.029  | 339                 |
|                                   | PP+nlcc | 5.119  | 1.018  | 334                 |
| B <sub>2</sub><br><sup>3</sup> Σ  | AE      | 3.032  | 3.855  | 1042                |
|                                   | PP      | 3.023  | 3.790  | 1037                |
|                                   | PP+nlcc | 3.034  | 3.852  | 1040                |
| C <sub>2</sub><br><sup>1</sup> Σ  | AE      | 2.353  | 7.251  | 1890                |
|                                   | PP      | 2.350  | 6.923  | 1877                |
|                                   | PP+nlcc | 2.355  | 7.223  | 1885                |
| N <sub>2</sub><br><sup>1</sup> Σ  | AE      | 2.068  | 11.602 | 2396                |
|                                   | PP      | 2.066  | 10.970 | 2388                |
|                                   | PP+nlcc | 2.069  | 11.497 | 2391                |
| O <sub>2</sub><br><sup>3</sup> Σ  | AE      | 2.273  | 7.591  | 1626                |
|                                   | PP      | 2.279  | 7.240  | 1613                |
|                                   | PP+nlcc | 2.279  | 7.506  | 1612                |
| F <sub>2</sub><br><sup>1</sup> Σ  | AE      | 2.614  | 3.397  | 1062                |
|                                   | PP      | 2.619  | 3.234  | 1058                |
|                                   | PP+nlcc | 2.618  | 3.375  | 1059                |
| LiH<br><sup>1</sup> Σ             | AE      | 3.032  | 2.643  | 1375                |
|                                   | PP      | 2.917  | 2.720  | 1320                |
|                                   | PP+nlcc | 3.037  | 2.597  | 1322                |
| FH<br><sup>1</sup> Σ              | AE      | 1.760  | 7.037  | 3995                |
|                                   | PP      | 1.764  | 6.915  | 3976                |
|                                   | PP+nlcc | 1.763  | 7.012  | 3979                |
| CO<br><sup>1</sup> Σ              | AE      | 2.128  | 12.967 | 2183                |
|                                   | PP      | 2.125  | 12.589 | 2164                |
|                                   | PP+nlcc | 2.128  | 12.900 | 2181                |
| average deviation                 | PP      | 0.026  | 0.235  | 15                  |
|                                   | PP+nlcc | 0.003  | 0.044  | 12                  |

### 3.3. Solids

Finally, in Tab. 5 we give a corresponding comparison for a few metals and semiconductors, relying on the results of AE LAPW calculations by Singh and collaborators<sup>26,60</sup> and of PP calculations by Fuchs *et al.*<sup>22</sup> Again the overall agreement is rather good as soon as nlccs are used. In most cases the error in the lattice constant is of the order of 0.01 – 0.03 Bohr, with GaAs being the only real exception. Linearly unscreened PPs, on the other hand, typically produce deviations of the order of 0.1 Bohr (apart from Al). The

Table 4. As Tab. 3 for second row dimers.

|                                   | mode    | $R_e$<br>[Bohr] | $D_e$<br>[eV] | $\omega_e$<br>[cm <sup>-1</sup> ] |
|-----------------------------------|---------|-----------------|---------------|-----------------------------------|
| Na <sub>2</sub><br><sup>1</sup> Σ | AE      | 5.673           | 0.883         | 162                               |
|                                   | PP      | 5.552           | 0.844         | 165                               |
|                                   | PP+nlcc | 5.662           | 0.876         | 161                               |
| Al <sub>2</sub><br><sup>3</sup> Σ | AE      | 4.650           | 1.982         | 348                               |
|                                   | PP      | 4.630           | 1.978         | 347                               |
|                                   | PP+nlcc | 4.644           | 1.989         | 348                               |
| Si <sub>2</sub><br><sup>3</sup> Σ | AE      | 4.283           | 4.040         | 490                               |
|                                   | PP      | 4.264           | 3.986         | 490                               |
|                                   | PP+nlcc | 4.271           | 4.062         | 493                               |
| P <sub>2</sub><br><sup>1</sup> Σ  | AE      | 3.570           | 6.225         | 798                               |
|                                   | PP      | 3.556           | 6.014         | 793                               |
|                                   | PP+nlcc | 3.565           | 6.217         | 799                               |
| S <sub>2</sub><br><sup>3</sup> Σ  | AE      | 3.576           | 5.876         | 719                               |
|                                   | PP      | 3.571           | 5.771         | 721                               |
|                                   | PP+nlcc | 3.572           | 5.899         | 723                               |
| Cl <sub>2</sub><br><sup>1</sup> Σ | AE      | 3.738           | 3.626         | 564                               |
|                                   | PP      | 3.736           | 3.560         | 564                               |
|                                   | PP+nlcc | 3.734           | 3.635         | 565                               |
| average                           | PP      | 0.030           | 0.080         | 1.8                               |
| deviation                         | PP+nlcc | 0.007           | 0.013         | 1.7                               |

cohesive energy is also consistently improved by the inclusion of nlccs. Here the errors are between 0.05 and 0.15 eV, which is only slightly larger than the deviations found for the diatomic molecules. The situation is somewhat less clear for the bulk modulus.

It seems worthwhile to emphasize that the comparison between AE and PP results is much more difficult in the case of solids than for diatomic molecules: While the same code and high quality basis sets have been employed for the AE and PP entries in Tabs. 3 and 4, the computational details of the AE and PP calculations of Tab. 5 are quite different (in particular, the basis sets). We point out that our own results for Aluminum are in excellent agreement with those by Fuchs *et al.*<sup>22</sup> if we restrict the integration over the Brillouin zone to the usual set of 28 special  $k$ -points. Our results in Tab. 5 have been obtained with 44 special  $k$ -points.

#### 4. Results Obtained with the Exact Exchange

In the present Section we contrast the LDA results of the previous Section with corresponding OPM data. This comparison reveals the reduced

Table 5. Equilibrium lattice constant  $a$ , cohesive energy  $E_{\text{coh}}$  and bulk modulus  $B$  of selected solids: PP versus AE-LAPW LDA results (pw – present work).

| system | mode                  | $a$<br>[Bohr] | $E_{\text{coh}}$<br>[eV/atom] | $B$<br>[GPa] |
|--------|-----------------------|---------------|-------------------------------|--------------|
| Na     | AE <sup>26</sup>      | 7.65          |                               | 9.2          |
|        | PP <sup>22</sup>      | 7.52          | 1.28                          | 8.7          |
|        | PP+nlcc <sup>22</sup> | 7.65          | 1.22                          | 9.1          |
| Al     | AE <sup>60</sup>      | 7.52          |                               | 84           |
|        | PP <sup>22</sup>      | 7.50          | 4.09                          | 83           |
|        | PP+nlcc <sup>22</sup> | 7.50          | 4.09                          | 85           |
|        | PP (pw)               | 7.47          | 4.08                          | 86           |
|        | PP+nlcc (pw)          | 7.48          | 4.08                          | 88           |
| Si     | AE <sup>60</sup>      | 10.22         | 5.28                          | 96           |
|        | PP <sup>22</sup>      | 10.17         | 5.34                          | 94           |
|        | PP+nlcc <sup>22</sup> | 10.19         | 5.32                          | 94           |
| Ge     | AE <sup>60</sup>      | 10.63         | 4.54                          | 78           |
|        | PP <sup>22</sup>      | 10.51         | 4.75                          | 73           |
|        | PP+nlcc <sup>22</sup> | 10.58         | 4.58                          | 71           |
|        | Expt. <sup>60</sup>   | 10.69         | 3.85                          | 77           |
| GaAs   | AE <sup>60</sup>      | 10.62         | 7.99                          | 74           |
|        | PP <sup>22</sup>      | 10.39         | 8.68                          | 79           |
|        | PP+nlcc <sup>22</sup> | 10.53         | 8.15                          | 75           |
|        | Expt. <sup>60</sup>   | 10.68         | 6.52                          | 76           |

influence of the nonlinear contributions to the core-valence interaction in the case of the exact exchange, but also points to the presence of a spurious long-range structure in the OPM-PPs. The origin of this tail and first attempts at corrective measures are discussed in detail.

#### 4.1. Atoms

The OPM-PP results obtained for atoms on the basis of the linear unscreening procedure described in Sec. 2 are included in Tabs. 1 and 2. For the  $s-p$  transfer energies one finds that the differences between linearly unscreened PP and AE OPM data are below 0.18 eV for all transitions considered. In the case of the transitions into the minority spin  $p$ -states the deviations are thus similar to those found for the linearly unscreened LDA-PPs. On the other hand, for the transitions into the high-spin excited states the deviations are roughly half as large as those of the LDA. Obviously the energy gain obtained by an increase of the spin-polarization is not overestimated as much as in the case of the LDA. This is a first indication that the core-

valence interaction is less important for the exact exchange than it is for the LDA.

This conclusion is corroborated by the analysis of the effect of non-sphericity. For the x-only OPM the difference between the AE ground state energy calculated from a spherically restricted density and that obtained with a nonspherical density is 0.140 eV in the case of Oxygen (see Tab. 2). The OPM-PP calculation on the basis of linear unscreening, on the other hand, predicts an energy gain of 0.137 eV, in much better agreement with the AE number than one finds for the LDA. This result is characteristic for all open-shell atoms considered.

#### **4.2. Diatomic Molecules**

The molecular results obtained with linearly unscreened OPM-PPs are listed in Tabs. 6 and 7. Two sets of OPM-PPs are compared: The first set has been constructed with the full OPM, the second is based on the KLI approximation<sup>41</sup> (the latter has been applied both in the molecular PP and in the AE reference calculations — all data in Tabs. 6 and 7 are strictly nonrelativistic). Comparing Tabs. 6, 7 with Tabs. 3, 4, one first of all notices that the average deviations found for the two types of OPM-PPs are of the same order of magnitude as the corresponding errors of the linearly unscreened LDA-PPs: In fact, bond lengths are better reproduced in the case of the OPM-PPs. On the other hand, the distribution of the error among the molecules is rather different from that found for the LDA. This is particularly obvious in the case of the dissociation energy for which  $N_2$  and  $P_2$  do not show the maximum deviations any more. The different pattern indicates that for the OPM-PPs the errors do not primarily originate from a poor description of spin-polarization (which would have to be corrected by nlccs). This observation is consistent with the reduced importance of core states for atomic  $s - p$  transfer energies of Al and Si and the energy gain resulting from nonsphericity in the case of open-shell atoms (see Sec. 4.1). However, the absolute size of the deviations between AE and PP dissociation energies is nevertheless substantial, e.g. for  $C_2$  or  $O_2$ . In addition, the differences between full OPM-PP and KLI-PP results are often as large as the differences between PP and AE data, in obvious contrast to the excellent agreement of KLI with full OPM results found so far in all AE calculations. For instance, for  $F_2$  the OPM-PP overestimates the dissociation energy by 0.1 eV, while the KLI-PP underestimates it by

Table 6. As Tab. 3 for exact exchange: PP-results obtained with LDA-PP, full OPM-PP and KLI-approximated OPM-PP versus AE data.<sup>59</sup>

|                 | mode   | $R_e$<br>[Bohr] | $D_e$<br>[eV] | $\omega_e$<br>[cm <sup>-1</sup> ] |
|-----------------|--------|-----------------|---------------|-----------------------------------|
| Li <sub>2</sub> | AE     | 5.266           | 0.168         | 338                               |
|                 | KLI-PP | 5.262           | 0.152         | 334                               |
|                 | OPM-PP | 5.262           | 0.169         | 337                               |
|                 | LDA-PP | 5.021           | 0.227         | 355                               |
| B <sub>2</sub>  | AE     | 3.068           | 0.608         | 972                               |
|                 | KLI-PP | 3.083           | 0.424         | 950                               |
|                 | OPM-PP | 3.074           | 0.580         | 967                               |
|                 | LDA-PP | 2.999           | 0.688         | 1027                              |
| C <sub>2</sub>  | AE     | 2.332           | 0.281         | 1933                              |
|                 | KLI-PP | 2.340           | 0.195         | 1908                              |
|                 | OPM-PP | 2.331           | 0.454         | 1940                              |
|                 | LDA-PP | 2.301           | 0.341         | 1979                              |
| N <sub>2</sub>  | AE     | 2.011           | 4.972         | 2736                              |
|                 | KLI-PP | 2.016           | 5.091         | 2718                              |
|                 | OPM-PP | 2.008           | 5.353         | 2760                              |
|                 | LDA-PP | 1.994           | 5.019         | 2769                              |
| O <sub>2</sub>  | AE     | 2.184           | 1.441         | 1981                              |
|                 | KLI-PP | 2.188           | 1.951         | 1981                              |
|                 | OPM-PP | 2.167           | 1.806         | 2047                              |
|                 | LDA-PP | 2.176           | 1.391         | 1990                              |
| F <sub>2</sub>  | AE     | 2.496           | -1.607        | 1283                              |
|                 | KLI-PP | 2.484           | -1.016        | 1323                              |
|                 | OPM-PP | 2.462           | -1.704        | 1346                              |
|                 | LDA-PP | 2.494           | -1.663        | 1286                              |
| LiH             | AE     | 3.037           | 1.483         | 1427                              |
|                 | KLI-PP | 3.049           | 1.416         | 1342                              |
|                 | OPM-PP | 3.065           | 1.447         | 1390                              |
|                 | LDA-PP | 2.844           | 1.646         | 1416                              |
| FH              | AE     | 1.694           | 4.203         | 4501                              |
|                 | KLI-PP | 1.697           | 4.188         | 4470                              |
|                 | OPM-PP | 1.695           | 4.189         | 4485                              |
|                 | LDA-PP | 1.692           | 4.175         | 4492                              |
| CO              | AE     | 2.080           | 7.530         | 2444                              |
|                 | KLI-PP | 2.086           | 7.558         | 2423                              |
|                 | OPM-PP | 2.078           | 7.792         | 2460                              |
|                 | LDA-PP | 2.058           | 7.649         | 2478                              |
| average         | KLI-PP | 0.008           | 0.180         | 27                                |
| absolute        | OPM-PP | 0.011           | 0.150         | 26                                |
| deviation       | LDA-PP | 0.066           | 0.074         | 24                                |

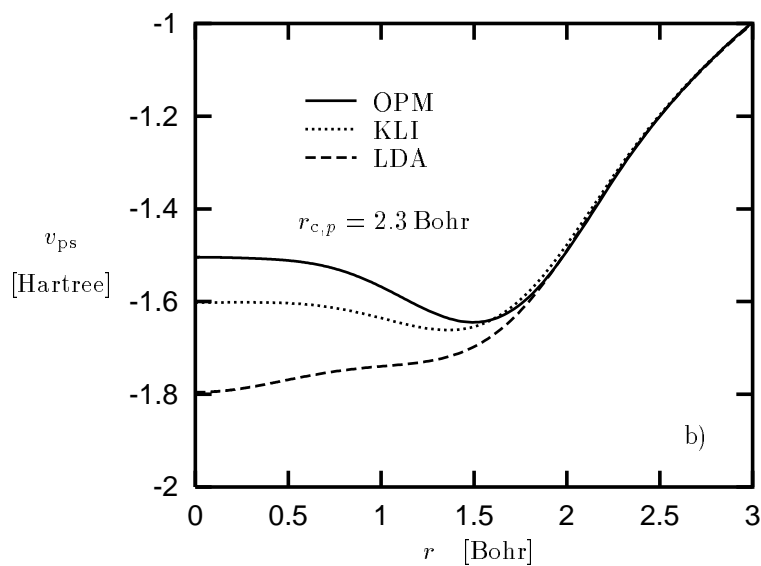
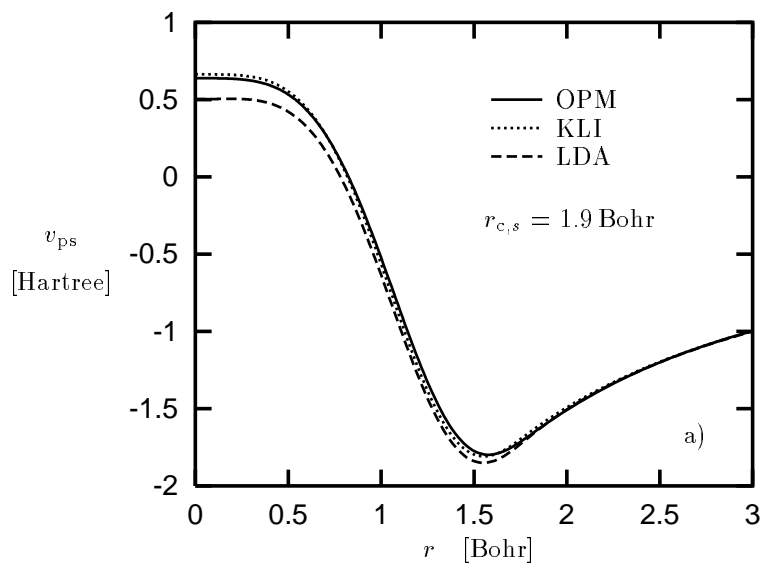
Table 7. As Tab. 6 for second row dimers.<sup>59</sup>

|                 | mode   | $R_e$<br>[Bohr] | $D_e$<br>[eV] | $\omega_e$<br>[cm <sup>-1</sup> ] |
|-----------------|--------|-----------------|---------------|-----------------------------------|
| Na <sub>2</sub> | AE     | 6.052           | -0.035        | 155                               |
|                 | KLI-PP | 6.041           | -0.064        | 150                               |
|                 | OPM-PP | 6.040           | -0.014        | 154                               |
|                 | LDA-PP | 5.513           | 0.043         | 173                               |
| Al <sub>2</sub> | AE     | 4.801           | 0.397         | 313                               |
|                 | KLI-PP | 4.823           | 0.200         | 302                               |
|                 | OPM-PP | 4.826           | 0.318         | 301                               |
|                 | LDA-PP | 4.665           | 0.438         | 326                               |
| Si <sub>2</sub> | AE     | 4.184           | 1.786         | 575                               |
|                 | KLI-PP | 4.189           | 1.532         | 568                               |
|                 | OPM-PP | 4.187           | 1.744         | 572                               |
|                 | LDA-PP | 4.091           | 1.907         | 589                               |
| P <sub>2</sub>  | AE     | 3.492           | 1.614         | 918                               |
|                 | KLI-PP | 3.497           | 1.199         | 903                               |
|                 | OPM-PP | 3.496           | 1.512         | 910                               |
|                 | LDA-PP | 3.400           | 1.779         | 936                               |
| S <sub>2</sub>  | AE     | 3.514           | 2.154         | 821                               |
|                 | KLI-PP | 3.529           | 1.750         | 805                               |
|                 | OPM-PP | 3.522           | 2.092         | 814                               |
|                 | LDA-PP | 3.466           | 2.276         | 835                               |
| Cl <sub>2</sub> | AE     | 3.727           | 0.715         | 613                               |
|                 | KLI-PP | 3.756           | 0.351         | 596                               |
|                 | OPM-PP | 3.746           | 0.676         | 603                               |
|                 | LDA-PP | 3.689           | 0.725         | 621                               |
| average         | KLI-PP | 0.014           | 0.277         | 12                                |
| absolute        | OPM-PP | 0.012           | 0.058         | 7                                 |
| deviation       | LDA-PP | 0.158           | 0.089         | 14                                |

0.6 eV. In order to understand the mechanism which is responsible for this behavior one has to analyze the OPM-PPs in more detail.

#### 4.3. Detailed Analysis of OPM Pseudopotentials: Al

As an example of the OPM-PPs obtained for second row atoms we analyze the potential for Aluminum. In Fig. 1.a-c the corresponding linearly unscreened  $s$ -,  $p$ - and  $d$ -PPs obtained with the RTM scheme<sup>52</sup> are plotted. For the construction of all three components the ground state configuration of Al,  $3s^2 3p_{1/2}^1$ , has been used. While this leads to a rather delocalized  $3d$ -orbital with an extremum at 6.5 Bohr, the  $d$ -state is nevertheless well bound (with an eigenvalue of  $-66$  mHartree). For comparison the PP obtained by use of the KLI approximation and the corresponding LDA-PPs are also



shown in Figs. 1.a-c. Overall, the  $s$  component of the OPM-PP is not very different from its LDA counterpart. One only observes an outward shift of

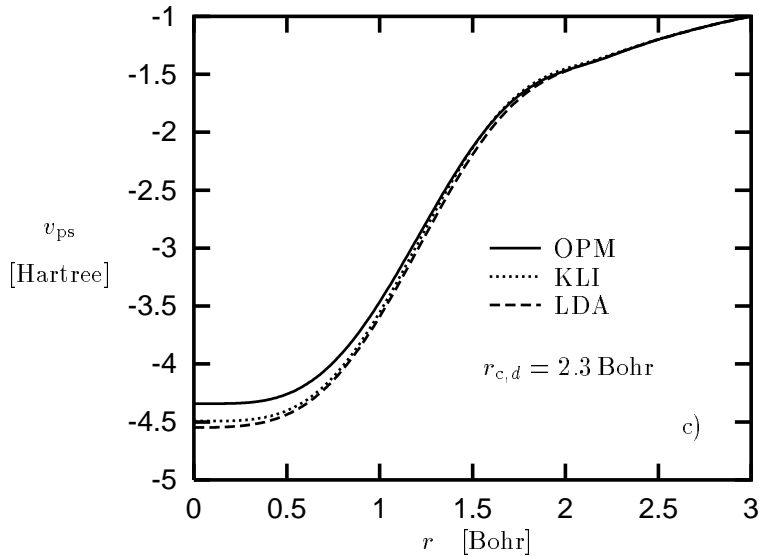


Fig. 1. Pseudopotentials for Al obtained with linear unscreening: OPM in comparison with LDA and KLI approximation (a: *s*-PP, b: *p*-PP, c: *d*-PP).

the minimum at 1.5 Bohr by 0.05 Bohr. This is consistent with the outward shift of the  $3s$  orbital whose  $r$ -expectation value increases from 2.54 Bohr to 2.59 Bohr, when going from the LDA to the OPM. Also, the  $s$ -component of the KLI-PP is rather close to the full OPM-PP. The  $p$ -component, on the other hand, reflects the more pronounced shell structure obtained with the exact exchange potential,<sup>40</sup> which requires a slightly enhanced separation of the valence shell from the core shells. Here the OPM-PP is substantially more repulsive than the LDA-PP, the KLI-approximated PP lies somewhere in between.

Figure 1 illustrates the differences between the three PPs in the core region, but does not really allow an examination of the valence regime. As already noted by Bylander and Kleinman,<sup>27</sup> the OPM-PPs contain a long-range component beyond the leading, electrostatic  $-Z_{\text{ion}}e^2/r$  term, which is not present in the case of the LDA. This long-range tail becomes obvious if the leading term is subtracted. In Fig. 2 we plot

$$rv_{\text{ps}}(r) + Z_{\text{ion}}e^2$$

for the  $p$ -PP of Aluminum, focusing on the asymptotic regime (beyond

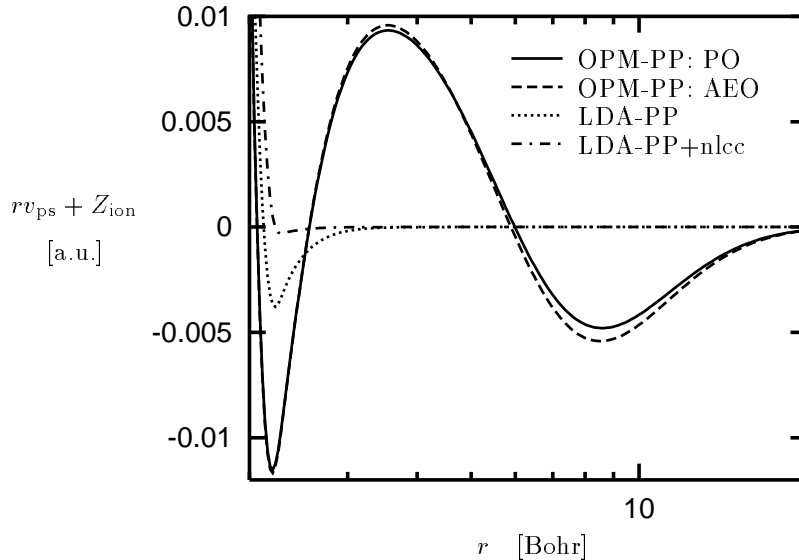


Fig. 2. Asymptotic behavior of OPM-PP for  $p$ -state of Al for different variants of linear unscreening: Unscreening with POs versus unscreening with AEOs in comparison to LDA-PP without and with nlcc.

the maximum  $r_c$  the  $s$ - and  $d$ -PPs are identical to the  $p$ -PP by construction). One observes some kind of damped oscillation of  $rv_{ps}(r)$  around  $-Z_{ion}e^2$ , which is not present in the corresponding LDA-PPs: While the LDA-PP without nlcc still shows a small structure close to the cutoff radius ( $r_{c,p} = 2.3$  Bohr), the LDA-PP including the nlcc demonstrates the ideal asymptotic behavior. The same type of oscillatory structure is found in the OPM-PPs of all first and second row atoms. In poly-atomic systems this tail leads to a small shift of the interaction energy between an ion at one center and the electrons around a second center. Depending on the separation of the two centers and the spatial distribution of the electrons this shift can be either attractive or repulsive. It is mainly this mechanism which is responsible for the different behavior of OPM- and LDA-PPs documented in Tabs. 3, 4, 6 and 7.

In order to investigate the long-range tail further a variant of the OPM-PP, which is obtained from linear unscreening with the AEOs, is shown in Fig. 2. In this case the OPM integral equation (17) is solved with a response function and an inhomogeneity in which only the valence AEOs are taken

into account (however,  $G_{nlj}$  is still evaluated via (21) in which completeness has been utilized implicitly). If one compares the linear unscreening with POs to that with AEOs one notices that both PPs are extremely similar in the asymptotic regime. The long-range structure is thus not due to an incomplete optimization of the POs. This implies that the inclusion of further subsidiary conditions in the PP construction, as e.g. the minimization of

$$\left| \int d^3r \frac{\phi_{\text{core}}^{\text{AE},\dagger}(\mathbf{r})}{|\mathbf{r} - \mathbf{r}'|} [\phi_{\text{valence}}^{\text{AE}}(\mathbf{r}) - \phi_{\text{valence}}^{\text{ps}}(\mathbf{r})] \right|,$$

does not eliminate the long-range structure, as long as linear unscreening is applied (this result is corroborated from a different perspective by an analysis of the multipole expansion of the OPM-PP in Appendix B).

In order to analyze the origin of the tail further we also plot five PPs obtained with different variants of nonlinear unscreening in Fig. 3. In the first

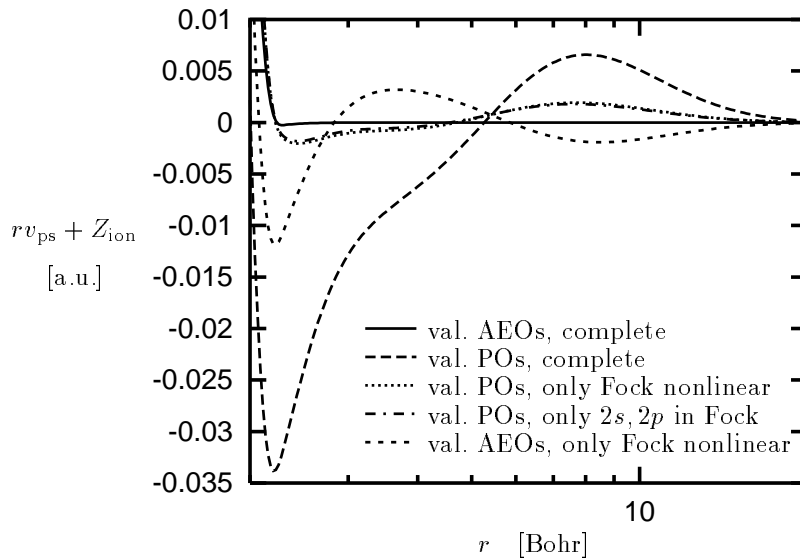


Fig. 3. Asymptotic behavior of OPM-PP for  $p$ -state of Al for different variants of nonlinear unscreening: Unscreening with full AE exchange potential, i.e. with core and valence AEOs (val. AEOs, complete), in comparison with standard combination of core AEOs plus valence POs (val. POs, complete) and three only partially nonlinear schemes, in which either all or the  $2s, 2p$  core AEOs are included in the inhomogeneity (19), but not in the kernel (18).

case, we subtract the complete AE exchange potential from the screened PPs (together with the valence AE Hartree potential). The result of this procedure is a PP which is completely free of long-range oscillations, very similar to the LDA-PP with nlcc of Fig. 2. This explicitly demonstrates that the core-valence interaction is responsible for the spurious tail. In PP applications, however, any nonlinear unscreening has to be based on a combination of the AE core states with the POs for the valence states, as only these are available in a poly-atomic calculation. Thus, for the second nonlinear unscreening variant, the exchange component of the unscreening potential is generated from the combination of AE core and PP valence orbitals, both in the kernel and in the inhomogeneity of the OPM integral equation. This procedure is conceptually closest to the standard nonlinear unscreening (9). In this case the resulting PP again shows a long-range structure, which, however, is quite different from the oscillatory behavior observed for linear unscreening, its absolute size being even larger.

In order to analyze the origin of this new structure we consider a third nonlinear unscreening variant: If one combines the AE core orbitals with the PP valence orbitals inside  $\delta E_x/\delta\varphi_k$ , but uses only the valence POs in the response function  $K$  and in the sum over the KS states in the inhomogeneity (19), most of the structure is eliminated (see Fig. 3). This demonstrates that the response components of the OPM integral equation are much more sensitive to the difference between POs and AEOs than the Fock integrals. On the other hand, the comparison of this partially nonlinear unscreening with the original linear unscreening shows that the long-range structure is mainly due to the nonlinearity of the Fock expression.

It remains to examine the question whether the inclusion of all core states in  $\delta E_x/\delta\varphi_k$  is required to eliminate the tail. Clearly, the Fock integrals between orbitals from neighbouring shells are larger than those between the valence and the innermost shell. In a fourth nonlinear unscreening variant only the  $L$ -shell is included in the evaluation of  $\delta E_x/\delta\varphi_k$ , while the  $K$ -shell is neglected. The resulting long-range structure remains essentially the same as the one found with inclusion of the  $K$ -shell (see Fig. 3). This partially nonlinear unscreening variant, including only the outermost core states in  $\delta E_x/\delta\varphi_k$ , appears to be the most appropriate nonlinear unscreening scheme.

On the other hand, even in this case a non-negligible spurious tail is present. At first glance, one might expect that further progress could be

achieved by an optimization of the valence POs. However, a final, fifth nonlinear unscreening variant demonstrates that some minor remnant of the spurious tail seems to be unavoidable. In this variant only AEOs are used, the sums over  $nlj$  in Eqs. (28), (29) are restricted to the valence states, but all core and valence states are included in  $\delta E_x/\delta\varphi_k$ . One again observes a substantial long-range structure (see Fig. 3). As any further optimization of the valence POs can only aim at the reproduction of additional features of the AEOs (as moments etc) this result leaves little hope to completely eliminate the tail in this fashion.

In addition, nonlinear unscreening is not a very attractive option in practice, in particular within the often used Plane-Wave-Pseudopotential (PWPP) scheme. A plane-wave representation of the core states requires extremely high energy cutoffs, even if one restricts oneself to the outermost core shell. On the other hand, if localized basis states are used for the representation of the core states the numerical evaluation of the Fock integrals between the valence orbitals and the core states requires enlarged spatial grids. In both cases the PP approach starts to lose its computational advantage over AE OPM calculations. Given the limited success of nonlinear unscreening in eliminating the spurious tail and the high computational demands of any OPM calculation, it seems that linear unscreening is to be preferred, in particular in PWPP-calculations.

As a consequence, the question arises how one can handle the unphysical long-range tail within the linear unscreening scheme. Kim and coworkers<sup>30</sup> suggested performing molecular OPM calculations on the basis of LDA-PPs. This scheme avoids all problems related to the spurious long-range tail from the very outset. However, the resulting dissociation energies are not consistently closer to the AE values than those obtained with the original OPM-PPs (see Tabs. 6 and 7). Moreover, the corresponding average deviations for  $R_e$  are much larger than those found with the OPM-PPs (or the consistent LDA approach). This result is in accordance with the general observation that only the consistent use of the same xc-functional in the PP construction and the poly-atomic calculation allows for accurate PP calculations.<sup>22</sup>

Bylander and Kleinman<sup>27</sup> suggested two strategies in order to correct the long-range tail. In their first approach the cutoff radii are optimized in order to suppress the non-electrostatic asymptotic tail as much as possible. However, Fig. 4 demonstrates that this method has little impact in the case

of Al. Increasing or reducing the cutoff radius of the  $s$ -PP by 0.4 Bohr does

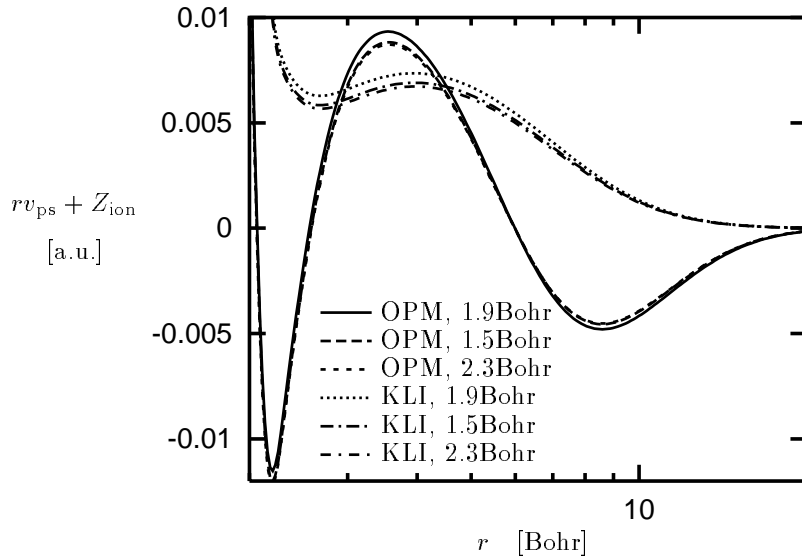


Fig. 4. Asymptotic behavior of OPM-PP for  $p$ -state of Al: Full OPM versus KLI approximation for different cutoff radii of the  $3s$ -state.

not really change the picture. Variation of the  $p$  cutoff radius has even less effect.

The same insensitivity to variation of  $r_c$  is found within the KLI approximation (see also Fig. 4). Apart from that the KLI long-range tail clearly differs from the OPM tail. While it is of the same magnitude, it does not show the oscillatory behavior of the OPM tail. This explains the differences between the spectroscopic constants calculated on the basis of OPM- and KLI-PPs.

#### 4.4. *A Posteriori Damping of Long-Range Structure*

As a second strategy Bylander and Kleinman suggested<sup>27</sup> damping the long-range structure *a posteriori*. The simplest form of damping which preserves the continuity of the first derivative of  $v_{ps}$  is given by

$$v_{ps}^{\text{damp}}(r) = \begin{cases} v_{ps}(r) & \text{for } r \leq r_d \\ [1 - f(r)](-Z_{\text{ion}}e^2/r) + f(r)v_{ps}(r) & \text{for } r \geq r_d \end{cases} \quad (34)$$

$$f_G(r) = \exp \left[ - \left( \frac{r - r_d}{l_d} \right)^2 \right]. \quad (35)$$

In view of the asymptotic behavior of the LDA-PP (see Fig. 2) a natural choice for the parameters in Eqs. (34), (35) is an onset radius  $r_d$  equal to the outermost cutoff radius among the occupied orbitals and a damping length  $l_d$  of roughly 1 Bohr. The molecular results obtained with this simple form of damped PPs are listed in Tabs. 8 and 9. For both the full OPM-PPs

Table 8. As Tab. 6 for various modified OPM-PPs with correct asymptotic behavior: Damped PP (D-KLI-PP, D-OPM-PP) versus selfconsistent PP (SC-OPM-PP).<sup>59</sup>

|                 | mode      | $R_e$<br>[Bohr] | $D_e$<br>[eV] | $\omega_e$<br>[cm <sup>-1</sup> ] |
|-----------------|-----------|-----------------|---------------|-----------------------------------|
| Li <sub>2</sub> | D-KLI-PP  | 5.262           | 0.153         | 334                               |
|                 | D-OPM-PP  | 5.262           | 0.169         | 337                               |
|                 | SC-OPM-PP | 5.257           | 0.171         | 337                               |
| B <sub>2</sub>  | D-KLI-PP  | 3.084           | 0.542         | 954                               |
|                 | D-OPM-PP  | 3.070           | 0.638         | 968                               |
|                 | SC-OPM-PP | 3.063           | 0.654         | 972                               |
| C <sub>2</sub>  | D-KLI-PP  | 2.338           | 0.148         | 1911                              |
|                 | D-OPM-PP  | 2.329           | 0.361         | 1934                              |
|                 | SC-OPM-PP | 2.323           | 0.379         | 1939                              |
| N <sub>2</sub>  | D-KLI-PP  | 2.014           | 4.865         | 2724                              |
|                 | D-OPM-PP  | 2.009           | 5.133         | 2744                              |
|                 | SC-OPM-PP | 2.003           | 5.142         | 2749                              |
| O <sub>2</sub>  | D-KLI-PP  | 2.186           | 1.482         | 1977                              |
|                 | D-OPM-PP  | 2.179           | 1.590         | 1988                              |
|                 | SC-OPM-PP | 2.182           | 1.466         | 1971                              |
| F <sub>2</sub>  | D-KLI-PP  | 2.498           | -1.602        | 1284                              |
|                 | D-OPM-PP  | 2.496           | -1.586        | 1283                              |
|                 | SC-OPM-PP | 2.498           | -1.641        | 1281                              |
| LiH             | D-KLI-PP  | 3.049           | 1.417         | 1342                              |
|                 | D-OPM-PP  | 3.051           | 1.453         | 1392                              |
|                 | SC-OPM-PP | 3.037           | 1.461         | 1393                              |
| FH              | D-KLI-PP  | 1.696           | 4.148         | 4472                              |
|                 | D-OPM-PP  | 1.696           | 4.164         | 4475                              |
|                 | SC-OPM-PP | 1.694           | 4.163         | 4479                              |
| CO              | D-KLI-PP  | 2.084           | 7.404         | 2427                              |
|                 | D-OPM-PP  | 2.078           | 7.679         | 2451                              |
|                 | SC-OPM-PP | 2.071           | 7.692         | 2456                              |
| average         | D-KLI-PP  | 0.006           | 0.068         | 21                                |
| absolute        | D-OPM-PP  | 0.004           | 0.073         | 10                                |
| deviation       | SC-OPM-PP | 0.005           | 0.067         | 11                                |

Table 9. As Tab. 8 for second row dimers.<sup>59</sup>

|                 | mode      | $R_e$<br>[Bohr] | $D_e$<br>[eV] | $\omega_e$<br>[cm <sup>-1</sup> ] |
|-----------------|-----------|-----------------|---------------|-----------------------------------|
| Na <sub>2</sub> | D-KLI-PP  | 6.032           | -0.059        | 152                               |
|                 | D-OPM-PP  | 6.070           | -0.037        | 152                               |
|                 | SC-OPM-PP | 6.013           | -0.018        | 155                               |
| Al <sub>2</sub> | D-KLI-PP  | 4.812           | 0.372         | 309                               |
|                 | D-OPM-PP  | 4.786           | 0.407         | 315                               |
|                 | SC-OPM-PP | 4.825           | 0.373         | 310                               |
| Si <sub>2</sub> | D-KLI-PP  | 4.186           | 1.731         | 570                               |
|                 | D-OPM-PP  | 4.173           | 1.815         | 578                               |
|                 | SC-OPM-PP | 4.184           | 1.790         | 576                               |
| P <sub>2</sub>  | D-KLI-PP  | 3.498           | 1.480         | 905                               |
|                 | D-OPM-PP  | 3.487           | 1.624         | 916                               |
|                 | SC-OPM-PP | 3.493           | 1.598         | 913                               |
| S <sub>2</sub>  | D-KLI-PP  | 3.523           | 2.070         | 814                               |
|                 | D-OPM-PP  | 3.511           | 2.182         | 822                               |
|                 | SC-OPM-PP | 3.515           | 2.175         | 822                               |
| Cl <sub>2</sub> | D-KLI-PP  | 3.735           | 0.657         | 611                               |
|                 | D-OPM-PP  | 3.725           | 0.711         | 615                               |
|                 | SC-OPM-PP | 3.729           | 0.709         | 615                               |
| average         | D-KLI-PP  | 0.009           | 0.063         | 6                                 |
| absolute        | D-OPM-PP  | 0.009           | 0.014         | 2                                 |
| deviation       | SC-OPM-PP | 0.011           | 0.015         | 2                                 |

and the KLI-approximated PPs one notices a marked improvement of the dissociation energies over the corresponding unmodified PPs. The errors in the bond length, on the other hand, are only moderately reduced<sup>b</sup>. Taking the LDA results of Tabs. 3 and 4 as reference data, the overall accuracy of the damped OPM-PPs is very satisfying. In fact, the average errors of the OPM-PPs are smaller than those found with the linearly unscreened LDA-PPs. This is another indication of the reduced importance of the core-valence interaction in the case of the exact exchange.

However, in view of Eqs. (34), (35) a question immediately arises concerning the sensitivity of poly-atomic results with respect to the damping function and the parameters chosen. In order to analyze this sensitivity we have performed PP calculations for both the Al dimer and bulk Al with different damping functions. In addition to the Gaussian damping (35), for

<sup>b</sup>Differences of less than 0.003 Bohr between the average deviations of two types of PP should not be considered as significant due to the dependence of the average deviations on the statistical sample.

which the damping parameters have been varied, we have considered power law damping, realized via a Padé function,

$$f_P(r) = \left[ 1 - \left( \frac{r - r_d}{l_d} \right)^2 \right]^{-1}. \quad (36)$$

The corresponding OPM-PPs are plotted in Fig. 5. While the power law

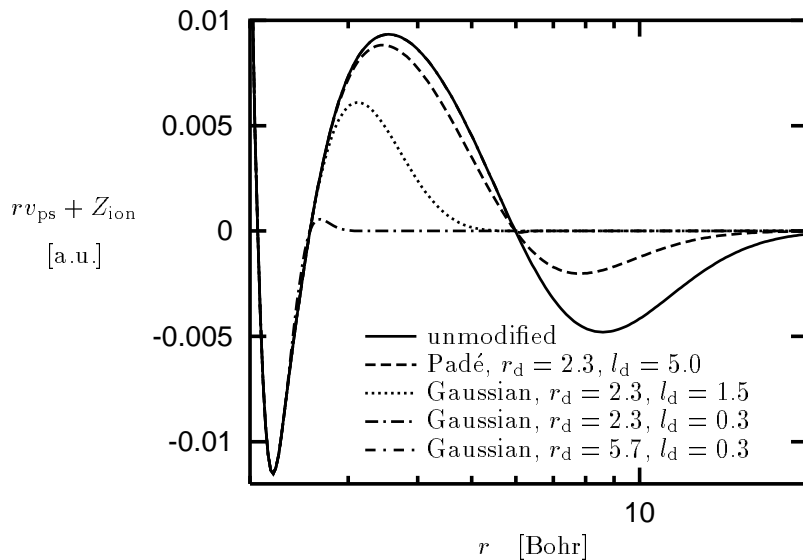


Fig. 5. OPM pseudopotential for  $p$ -state of Al: Various damping schemes for long-range structure (linear unscreening).

damping with  $l_d = 5$  Bohr just reduces the amplitudes of the oscillations, the Gaussian damping with short damping length  $l_d = 0.3$  Bohr allows their complete elimination. This can either be done for large  $r_d$ , eliminating only the minimum around  $r = 8.4$  Bohr, or for small  $r_d$ , so that also the maximum around  $r = 3.5$  Bohr is taken out (in Fig. 5 the curve corresponding to the former PP is almost hidden by other potentials). A smoother Gaussian ( $l_d = 1.5$  Bohr) leaves part of the inner structure intact.

The spectroscopic constants obtained with the different variants of damping for  $\text{Al}_2$  are listed in Tab. 10. The different damping functions give similar results, in consistency with Tab. 7. The bond length varies by less than

Table 10. Bond length  $R_e$ , dissociation energy  $D_e$  (including zero-point energy) and harmonic frequency  $\omega_e$  of  $\text{Al}_2$ : Various damping variants in comparison with unmodified PP.<sup>59</sup>  $E_{xc}$  denotes the functional used in the molecular PP calculation.

| $E_{xc}$            | damping function | $r_d$<br>[Bohr] | $l_d$<br>[Bohr] | $R_e$<br>[Bohr] | $D_e$<br>[eV] | $\omega_e$<br>[ $\text{cm}^{-1}$ ] |
|---------------------|------------------|-----------------|-----------------|-----------------|---------------|------------------------------------|
| exact $E_x$         | unmodified       |                 |                 | 4.826           | 0.318         | 301                                |
| exact $E_x$         | Padé             | 2.3             | 5.0             | 4.817           | 0.316         | 302                                |
| exact $E_x$         | Gaussian         | 5.7             | 0.3             | 4.813           | 0.290         | 303                                |
| exact $E_x$         | Gaussian         | 2.3             | 1.5             | 4.793           | 0.381         | 311                                |
| exact $E_x$         | Gaussian         | 2.3             | 0.3             | 4.773           | 0.429         | 318                                |
| LDA                 | unmodified       |                 |                 | 4.780           | 1.818         | 323                                |
| LDA                 | Gaussian         | 2.3             | 0.3             | 4.734           | 1.934         | 340                                |
| Expt. <sup>61</sup> |                  |                 |                 | 4.660           | 1.57          | 350                                |

0.05 Bohr even between the most extreme choices, the dissociation energy by less than  $0.14 \text{ eV}$  and the vibrational frequency by only  $18 \text{ cm}^{-1}$ . On the other hand, these differences are of the same size as the deviations of the unmodified PP values from the AE data, a fact which questions the usefulness of the damping approach.

The corresponding results for bulk Al are given in Tab. 11. In order to

Table 11. Equilibrium lattice constant  $a$ , cohesive energy  $E_{\text{coh}}$  and bulk modulus  $B$  of fcc Al: Various damping variants in comparison with unmodified PP<sup>59</sup> (the experimental values have been taken from<sup>22</sup>).  $E_{xc}$  denotes the functional used in the bulk PP calculation.

| $E_{xc}$    | damping function | $r_d$<br>[Bohr] | $l_d$<br>[Bohr] | $w_{ps,d}(0)$<br>[a.u.] | $a$<br>[Bohr] | $E_{\text{coh}}$<br>[eV/atom] | $B$<br>[GPa] |
|-------------|------------------|-----------------|-----------------|-------------------------|---------------|-------------------------------|--------------|
| LDA         | unmodified       |                 |                 | -3.478                  | 7.04          | 6.50                          | 139.2        |
| LDA         | Padé             | 2.3             | 5.0             | -0.754                  | 7.60          | 4.23                          | 82.5         |
| LDA         | Gaussian         | 2.3             | 0.3             | -0.526                  | 7.64          | 3.98                          | 80.4         |
| LDA         | Gaussian         | 2.3             | 1.5             | -0.218                  | 7.72          | 3.80                          | 72.1         |
| LDA         | Gaussian         | 5.7             | 0.3             | 0.444                   | 7.89          | 3.39                          | 56.0         |
| LDA         | SC-OPM-PP        |                 |                 | -0.689                  | 7.75          | 3.82                          | 72.7         |
| exact $E_x$ | SC-OPM-PP        |                 |                 | -0.689                  | 7.79          | 1.37                          | 70.6         |
| Expt.       |                  |                 |                 |                         | 7.65          | 3.39                          | 77.3         |

enhance the efficiency, the LDA has been used for the bulk calculations.<sup>56</sup> This procedure is legitimate for the present purpose as we are only interested in the variation of the bulk results with the damping scheme chosen, but not in absolute numbers. In fact, applying the same approach to  $\text{Al}_2$  gives a spread of results in very good agreement with that found for the

molecular OPM calculations (see Tab. 10). It is obvious from Tab. 11 that the sensitivity of the bulk data to the asymptotic form of the PPs is much higher than that of the molecular properties. The unmodified PP gives a lattice constant which is roughly 0.6 Bohr shorter than those found with the damped PPs and the experimental value of 7.65 Bohr. It is this point which definitively demands a modification of the OPM-PP scheme, in spite of the acceptable performance for diatomic molecules. Unfortunately, the spread of results among the various damped PPs is also not negligible: While it is smaller than the 0.6 Bohr difference between the set of damped PPs and the unmodified PP, its absolute size of about 0.3 Bohr is substantial. Even if one discards the somewhat extreme Gaussian damping with  $r_d = 5.7$  Bohr a spread of 0.12 Bohr remains.

The sensitivity of the cohesive properties to the long-range tail is most easily understood if one examines the PPs in momentum space,

$$w_{\text{ps},l}(|\mathbf{k}|) = \int d^3r \exp(i\mathbf{k} \cdot \mathbf{r}) \left[ v_{\text{ps},l}(r) + \frac{Z_{\text{ion}}e^2}{r} \right], \quad (37)$$

where again the purely electrostatic part of  $v_{\text{ps},l}$  has been subtracted. In  $w_{\text{ps},l}(k)$  the long-range tail of the OPM-PPs manifests itself mainly as a small dip at  $k = 0$  (see Fig. 6). However,  $k = 0$  and its immediate vicinity do not contribute to the total KS potential in a solid and thus do not affect the electronic structure (for Al with a lattice constant  $a$  of 7.5 Bohr the minimum reciprocal lattice vector  $|\mathbf{G}_{\text{min}}|$  equals  $1.45 \text{ Bohr}^{-1}$ ). On the other hand,  $w_{\text{ps},l}(k = 0)$  does affect the cohesive properties via the long-range component of the total energy,<sup>3</sup>

$$E_{\text{ext}}^{\text{long-range}} = \frac{N_{\Omega}}{\Omega} \sum_{j \in \Omega} w_{\text{ps},L}^j(k = 0), \quad (38)$$

where  $\Omega$  denotes the unit cell,  $j$  labels the atoms in  $\Omega$ ,  $N_{\Omega}$  is the total number of electrons in  $\Omega$  and  $v_{\text{ps},L}^j$  is the local component of the PP chosen for atom  $j$ . Tab. 11 directly reflects the dependence of  $E_{\text{ext}}^{\text{long-range}}$  on  $w_{\text{ps},L}(k = 0)$ ,  $E_{\text{ext}}^{\text{long-range}} \sim w_{\text{ps},L}(0)/a^3$ , i.e. the large number of neighbouring atoms which experience the long-range tail. Moreover, due to the fact that the unmodified OPM-PPs oscillate around  $-Z_{\text{ion}}e^2/r$  the value of  $w_{\text{ps},L}(k = 0)$  results from a subtle balance between positive and negative contributions, which can easily be influenced by the form of the damping function (see Tab. 11). In spite of the obvious improvement resulting from damping, the high sensitivity of  $E_{\text{tot}}(a)$  to the detailed form of the damping

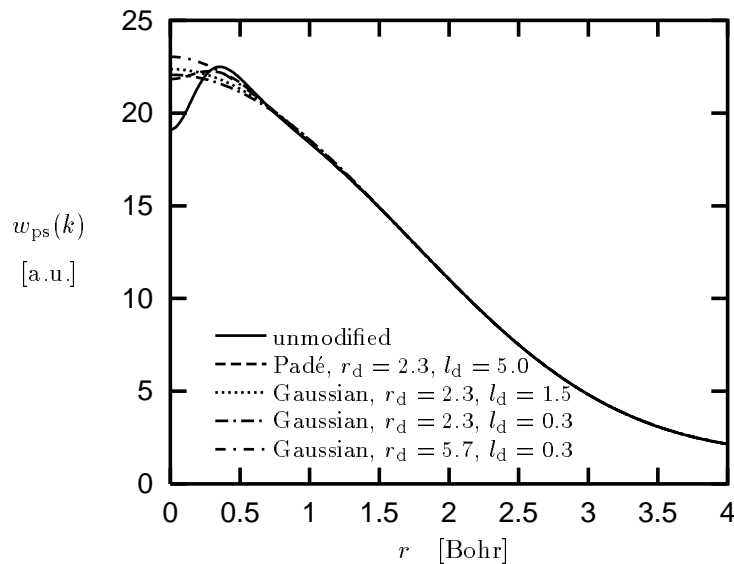


Fig. 6. As in Fig. 5 in momentum space.

prescription introduces some arbitrariness into OPM results for structural parameters.

### 5. Selfconsistent Normconserving Pseudopotentials

If one wants to avoid *a posteriori* damping of the undesired long-range structure the PP construction itself has to be modified. Provided that one insists on using the standard OPM to generate  $v_x[n_{v,ps}]$  from the POs, one must give up the strict identity of the POs with the AEOs and thus the identity of the screened PPs with the total AE potential (in the valence region). A modified PP construction scheme could work as follows:<sup>53</sup>

- (1) One first applies the standard (R)TM procedure with the standard AE orbitals and potentials. This yields a set of POs, the corresponding pseudodensity  $n_{v,ps}$ , the screened PPs  $v_{ps,lj}^{sc}$  and the unscreening potentials  $v_H[n_{v,ps}]$  and  $v_x[n_{v,ps}]$ . These quantities provide the starting point for an iterative process.
- (2) In the next step one sets up a modified reference potential  $v_s^{mod}$  which will take the place of the original AE potential in the subsequent PP

construction. As one wants the resulting PPs to be free of any spurious tail, the asymptotic behavior of  $v_s^{\text{mod}}$  cannot be identical with that of the AE potential. A suitable form for the modified reference potential is given by

$$v_s^{\text{mod}}(r) = v_s^{\text{AE}}(r) - v_{\text{H}}([n_{\text{v}}^{\text{AE}}], r) - v_{\text{xc}}([n^{\text{AE}}], r) + v_{\text{H}}([n_{\text{v,ps}}], r) + v_{\text{xc}}([n_{\text{v,ps}}], r), \quad (39)$$

where  $n_{\text{v}}^{\text{AE}}$  denotes the AE valence density,  $n^{\text{AE}} = n_{\text{c}}^{\text{AE}} + n_{\text{v}}^{\text{AE}}$ . In  $v_s^{\text{mod}}$  the original AE long-range tail is substituted by the long-range tail of the unscreening potential in such a way that  $v_s^{\text{mod}} - v_{\text{H}}[n_{\text{v,ps}}] - v_{\text{xc}}[n_{\text{v,ps}}]$  has the correct asymptotic behavior:  $v_s^{\text{AE}} - v_{\text{H}}[n_{\text{v}}^{\text{AE}}] - v_{\text{xc}}[n^{\text{AE}}]$  has exactly the desired asymptotic form (see Fig. 3). The form of  $v_s^{\text{mod}}$  for  $r < r_{\text{c},l}$ , on the other hand, is irrelevant for the following.

- (3) Next one calculates a set of modified reference orbitals  $\varphi_{nlj}^{\text{mod}}$  on the basis of  $v_s^{\text{mod}}$ . At this point it is important to realize that the (R)TM scheme only uses the form of the reference (AE) orbitals in the valence region. Suitable reference orbitals can thus be obtained by inward integration of the radial differential equations with  $v_s^{\text{mod}}$ , restricting the energy parameters (eigenvalues) to the original AE values and requiring the norm of  $\varphi_{nlj}^{\text{mod}}$  in the valence region to be identical with that of the original AE orbital. Due to these conditions and the fact that  $v_s^{\text{mod}}$  is dominated by the  $-e^2/r$  behavior of the exchange component in  $v_s^{\text{AE}}$ , the resulting  $\varphi_{nlj}^{\text{mod}}$  are extremely close to the AEOs for  $r > r_{\text{c},l}$ .
- (4) Now one repeats the (R)TM procedure, using  $v_s^{\text{mod}}$  as reference potential and  $\varphi_{nlj}^{\text{mod}}$  as reference orbitals. As a result of this step one has new, somewhat modified POs, new screened PPs  $v_{\text{ps},lj}^{\text{sc},(1)}$  and new unscreening potentials  $v_{\text{H}}[n_{\text{v,ps}}^{(1)}]$  and  $v_{\text{xc}}[n_{\text{v,ps}}^{(1)}]$  (for the complete range of  $r$ ).
- (5) Now one iterates the steps 2-4 until selfconsistency is achieved, i.e. until the maximum difference between  $v_{\text{ps},lj}^{\text{sc},(i-1)}$  and  $v_{\text{ps},lj}^{\text{sc},(i)}$  becomes smaller than some suitable accuracy requirement.
- (6) Finally, one constructs the unscreened PPs by subtraction of the converged valence Hartree and xc-potential from the converged screened PPs,

$$v_{\text{ps},lj}(r) = v_{\text{ps},lj}^{\text{sc},(i)}(r) - v_{\text{H}}([n_{\text{v,ps}}^{(i)}], r) - v_{\text{xc}}(n_{\text{v,ps}}^{(i)}, r). \quad (40)$$

As  $v_{\text{ps},lj}^{\text{sc}}$  is identical to  $v_s^{\text{mod}}$  in the valence region the unscreened PP is free of any non-electrostatic long-range tail. The selfconsistent ap-

plication of this unscreened PP to the atomic ground state correctly reproduces the original AE eigenvalues.

The reason for the usefulness of this selfconsistent procedure lies in the fact that the requirements for the modified reference orbitals force them to be almost identical with the AEOs. Thus  $v_{xc}[n_{v,ps}^{(i)}]$  is essentially fixed and the iteration just serves to produce a reference potential which is consistent with these modified reference orbitals and at the same time has exactly the same non-electrostatic tail as  $v_{xc}[n_{v,ps}^{(i)}]$ . It seems worthwhile to emphasize that the selfconsistent scheme is only based on quantities known from the standard PP construction, so that no new parameters need to be introduced. We remark that variants of this scheme, as e.g. use of

$$v_s^{\text{mod}}(r) = v_s^{\text{AE}}(r) - v_x([n^{\text{AE}}], r) + v_x([n_{v,ps}], r),$$

in the iteration, give very similar PPs as only  $v_x[n_{v,ps}]$  has a sizable long-range component.

The unscreened PP for Al resulting from the selfconsistent procedure (SC-OPM-PP) is shown in Figs. 7 and 8. All components of the SC-OPM-

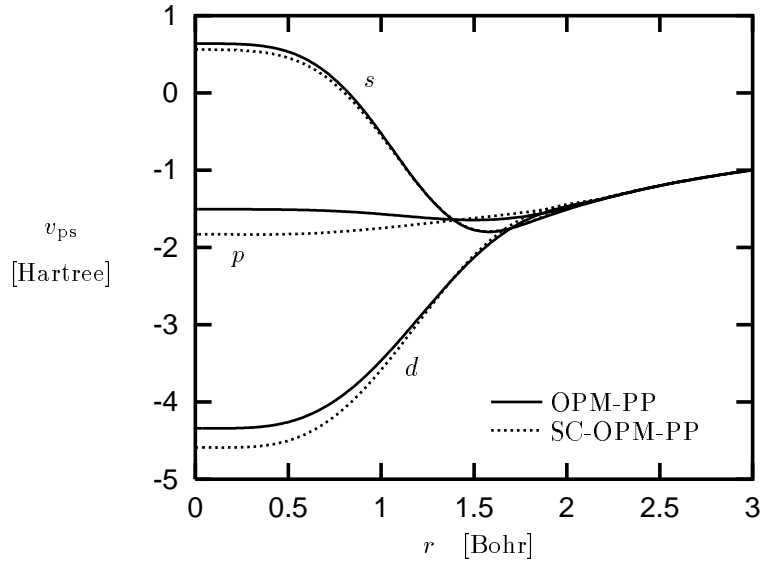


Fig. 7. OPM-PP for Al: Selfconsistent versus unmodified PP.

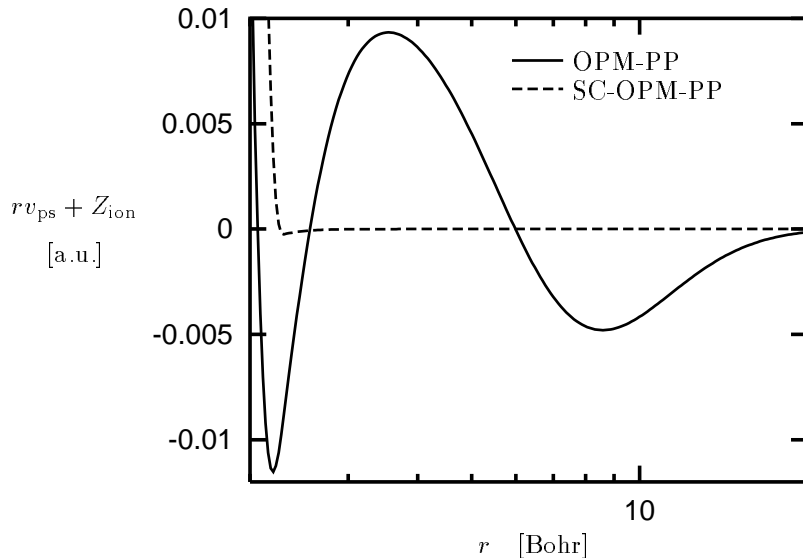


Fig. 8. Asymptotic behavior of OPM-PP for  $p$ -state of Al: Selfconsistent versus unmodified PP.

PP are slightly more attractive than their unmodified counterparts, in particular the  $p$ -component. The asymptotic behavior of the SC-OPM-PP is identical with that obtained from nonlinear unscreening with the AE exchange potential (Fig. 3). The cohesive properties of Aluminum obtained with this PP are included in Tab. 11. Using the LDA for the PWPP-calculation, rather realistic values emerge for both the lattice constant and the bulk modulus. A bulk calculation with the exact exchange (within the KLI approximation), on the other hand, yields a somewhat larger lattice constant of 7.79 Bohr and a somewhat smaller bulk modulus of 71 GPa. As no AE OPM calculation for bulk Al is available so far, one can only compare this result with LDA data and with experiment. Of course, one should not expect an x-only calculation to reproduce the cohesive properties of a metal. One can nevertheless indirectly draw some conclusion from this comparison by utilization of the corresponding information for the Al dimer: One observes that for the bulk the differences between the SC-OPM-PP results and the experimental data are similar to those between the AE OPM results for  $\text{Al}_2$  and the experimental dimer data.<sup>61</sup> In both cases the equilibrium separation is overestimated by 0.14 Bohr and the curvature of

the energy surface is underestimated by roughly 10%. This similarity can be interpreted as a confirmation of the quality of the SC-OPM-PP result.

In contrast to the bulk situation, a direct comparison with AE data is possible in the molecular case. The spectroscopic constants found with the SC-OPM-PPs for diatomic molecules are given in Tabs. 8 and 9. For all molecules the SC-OPM-PP data are very close to the damped OPM-PP values, so that the average deviations of both schemes are also very similar. The selfconsistent PP construction scheme thus represents a clear improvement over the straight (R)TM scheme, the resulting average deviations being roughly half as large. The overall level of accuracy is almost as high as that of the LDA-PPs with nlccs<sup>c</sup>.

## 6. Concluding Remarks

Due the nonlocality of the exact exchange the core-valence interaction introduces a non-electrostatic component in the asymptotic behavior of the ionic PP, as long as linear unscreening is applied. Although this spurious long-range tail decays much faster than  $1/r$ , it effectively acts like a small additional “ionic” force between two neighbouring atoms in a molecule or the bulk. As the spurious tail oscillates with the separation of the atoms, this force can either be attractive or repulsive, so that in different chemical environments either an erroneous bond length reduction or an increase can be observed. As the range of the tail is roughly 20 Bohr, not only nearest neighbours experience it. As a consequence, the importance of the spurious tail increases with the number of neighbours in the 20 Bohr cell, so that bulk results are more affected than those for small molecules.

The origin of the non-electrostatic tail immediately suggests the use of a nonlinear unscreening scheme in order to resolve this problem. Unfortunately, it turns out that only an unscreening with the full AE exchange potential completely eliminates the tail. In practice, one thus has to rely on some form of linear unscreening.

We have verified that the *a posteriori* damping of the spurious tail suggested by Bylander and Kleinman<sup>27</sup> consistently improves PP results on the basis of the exact exchange. However, this procedure introduces new

---

<sup>c</sup>It should be noted that the concept of selfconsistent PPs does not work quite as well in the case of the KLI approximation. Here the results for the second row dimers are significantly less accurate.

parameters into the PPs which lead to some ambiguity of the final results for poly-atomic systems, in particular for solids. As an alternative, we have outlined a modified PP construction scheme which is free of additional parameters. In this scheme the screened PP is determined in a selfconsistent fashion which guarantees that the final unscreened PP has the correct asymptotic behavior. The spectroscopic constants obtained with these PPs are as close to the corresponding AE OPM data as those of the damped OPM-PPs. The average deviations found for the selfconsistent PPs are significantly lower than those resulting from LDA calculations with linearly unscreened PPs. In fact, the errors are almost as low as those obtained for LDA-PPs which include nlccs. This indicates that, apart from being responsible for the spurious tail, the core-valence interaction is less important in the case of the OPM. The combination of linear unscreening with the selfconsistent generation of PPs thus provides an appropriate basis for PP calculations with the exact exchange.

### Acknowledgments

The authors wish to express their thanks to N. Chetty and M. Weinert for making their plane-wave-pseudopotential code BEST (Brookhaven Electronic STructure) available, which has been used as basis for the bulk OPM calculations. We would like to thank T. Auth and U. Lechner for carefully reading this manuscript. Financial support by the Deutsche Forschungsgemeinschaft (grant Dr 113/20-3) is gratefully acknowledged.

### Appendix A. Technical Details

All PPs used for this study have been generated from the relativistic atomic ground state configuration, applying finite differences methods and radial grids of 1600 mesh points. An accurate normalization of the OPM exchange potential has been ensured, both in the AE calculation and in the unscreening procedure, relying on the analytic form of  $v_x$  for large  $r$ .<sup>36</sup> In the case of the LDA<sup>56</sup> the Hamann prescription<sup>18</sup> has been utilized for unbound states, i.e. for the unoccupied  $3d$  orbitals of the second row atoms. The cutoff radii used for this study are listed in Tab. 12. Rather hard values have been chosen in order to ensure converged PP results.

For molecular OPM calculations the accurate KLI approximation<sup>41</sup> to Eqs. (17)–(21) proved to be an advantage.<sup>48</sup> The semianalytical KLI ap-

Table 12. Cutoff radii used in this work.

| atom | $r_c$ [Bohr] |     |     | $r_{nlcc}$ [Bohr] |
|------|--------------|-----|-----|-------------------|
|      | $s$          | $p$ | $d$ |                   |
| Li   | 2.8          | 3.0 | —   | 1.2               |
| B    | 1.3          | 1.3 | —   | 0.6               |
| C    | 1.2          | 1.1 | —   | 0.4               |
| N    | 1.1          | 1.0 | —   | 0.3               |
| O    | 1.0          | 0.9 | —   | 0.25              |
| F    | 0.6          | 0.5 | —   | 0.2               |
| Na   | 2.7          | 2.7 | 2.7 | 2.0               |
| Mg   | 1.9          | 2.3 | 2.3 | 1.2               |
| Al   | 1.9          | 2.3 | 2.3 | 1.0               |
| Si   | 1.8          | 2.0 | 2.0 | 1.0               |
| P    | 1.7          | 1.7 | 1.7 | 0.8               |
| S    | 1.4          | 1.5 | 1.5 | 0.7               |
| Cl   | 1.2          | 1.2 | 1.2 | 0.6               |

proximation allows the use of larger basis sets than the numerically much more involved full OPM. As a consequence, the KLI approximation in practice usually provides molecular ground state energies which are lower than those obtained with the full OPM in combination with more moderately sized basis sets.<sup>48</sup> The ground state energy is much more sensitive to the size of the basis set used than to the small differences between the OPM and the KLI exchange potential. We have thus always used the KLI approximation in the molecular and bulk OPM calculations.

For all molecular calculations prolate-elliptic coordinates and a Hyllebras-type two-center basis set have been employed (for the details see Ref. 48). In this approach the dominating source of error are the core orbitals. The representation of these rather localized orbitals requires many two-center basis functions and numerical integrals involving the core orbitals require many grid points in the core region. A measure for the ability of the two-center basis set to represent core orbitals is the variation of the ground state energies of the individual atoms in a molecule with the internuclear distance  $R$ . For all systems considered this variation was below 0.02 mHartree over the complete range of  $R$  required for the determination of the equilibrium separation. A measure of the quality of the grid is the associated absolute accuracy of the atomic ground state energies which can be checked by comparison with finite differences results. Even for the heaviest atoms the absolute accuracy was better than 0.03 mHartree in the

case of the LDA and of the order of 1 mHartree in the case of the exact exchange (which requires integrations over the Coulomb interaction). This error reduces to 0.2 mHartree for our PP calculations in which somewhat smaller basis set and grid sizes have been utilized. These core-related errors largely cancel in the energy surface

$$E_b(R) = E_{\text{tot}}[\text{XY}](R) - E_{\text{tot}}[\text{X}](R) - E_{\text{tot}}[\text{Y}](R),$$

if the atomic reference energies  $E_{\text{tot}}[\text{X}](R)$  are evaluated with the same basis set and grid as used in the molecular calculations. We have consistently used this approach, so that  $E_b(R)$  is one to two orders of magnitude more accurate than the individual  $E_{\text{tot}}(R)$ <sup>d</sup>. Finally, in order to obtain the spectroscopic parameters, the numerical values of  $E_b(R)$  have been fitted to a Morse potential, using 10 or more  $R$ -values. Taking all sources of numerical inaccuracies together, the resulting molecular bond lengths are converged to better than 0.002 Bohr, the dissociation energies are correct within 0.002 eV and vibrational frequencies within 10 cm<sup>-1</sup> (for given PP).

For the bulk calculations of Aluminum plane-wave basis sets with energy cutoffs of 25–35 Hartree have been used. The integrations over the Brillouin zone have been performed with the Monkhorst-Pack technique,<sup>62</sup> using 44 special  $k$ -points.

## Appendix B. Multipole Expansion of OPM Pseudopotential

The fact that the asymptotic structure of the OPM-PP for Aluminum is not very sensitive to the differences between the POs and AEOs can be understood more easily if one takes a closer look at the asymptotically dominant components of the PP. As the AEOs and POs are identical for  $r > r_c$  and have the same norm in the regime  $r < r_c$  their monopole moments are identical. On the other hand, their quadrupole moments differ slightly due to the fact that

$$\int_0^{r_c} dr r^2 |\varphi_{nlj}^{\text{AE}}(r)|^2 \neq \int_0^{r_c} dr r^2 |\varphi_{ps,lj}(r)|^2.$$

Consequently, the AE and PP solutions of (17) have in general different quadrupole components (the same holds for higher multipole moments if

<sup>d</sup>For open-shell atoms nonspherical potentials and densities have been applied for the evaluation of  $E_{\text{tot}}[\text{X}](R)$ .

they are present),

$$\begin{aligned}
 v_x(r \rightarrow \infty) &\sim -e^2 \sum_{L=0}^{\infty} \left\{ \alpha_{nlj}^{(L)} \frac{1 + (-1)^L}{2} + \frac{2j + 1 - \Theta_{nlj}}{2j} \delta_{L0} \right\} \\
 &\quad \times \int_0^{\infty} dr' \frac{r'^L}{r^{L+1}} |\phi_{nlj}(r')|^2 \\
 &\sim -\frac{e^2}{r} - \frac{e^2}{r^3} \alpha_{nlj}^{(2)} \int_0^{\infty} dr' r'^2 |\phi_{nlj}(r')|^2
 \end{aligned} \tag{41}$$

$$\alpha_{nlj}^{(L)} = (\Theta_{nlj} - 1) \frac{2j + 1}{2j} \frac{C(j \ 1/2 \ j \ -1/2 \ | \ L \ 0)^2}{(2L + 1)} \geq 0. \tag{42}$$

Here  $C$  denotes a Clebsch-Gordan coefficient,  $\phi_{nlj}$  is the most weakly bound occupied orbital and  $\Theta_{nlj}$  is its occupation (for a derivation see the Appendices of<sup>36</sup>). This leads to a quadrupole component in the unscreened PP,

$$v_{\text{ps},lj}(r \rightarrow \infty) \sim -\frac{Z_{\text{ion}} \epsilon^2}{r} - \frac{\epsilon^2}{r^3} \alpha_{nlj}^{(2)} \int_0^{r_c} dr' r'^2 \left[ |\phi_{nlj}^{\text{AE}}(r')|^2 - |\phi_{\text{ps},lj}(r')|^2 \right],$$

as long as  $\alpha_{nlj}^{(2)} \neq 0$ . For the relativistic  $3s^2 3p_{1/2}^1$  ground state of Al, however,  $\alpha_{nlj}^{(2)}$  vanishes, so that the PP discussed in Sec. 4.3 does not suffer from this deficiency (the quadrupole term would be present in a strictly nonrelativistic treatment in which the standard  $m$ -average for open subshells introduces a  $p_{3/2}$  component in  $v_x$ ). The long-range structure in the OPM-PP for Al is thus not due to an inaccurate quadrupole component in the valence exchange potential as one might have expected.

## References

1. See e.g. R. M. Dreizler and E. K. U. Gross, *Density Functional Theory*, (Springer, Berlin, 1990); J. F. Dobson, G. Vignale and M. P. Das (eds.), *Electronic Density Functional Theory*, (Plenum, New York, 1998).
2. R. Car and M. Parrinello, *Phys. Rev. Lett.* **55**, 2471 (1985).
3. M. C. Payne, M. P. Teter, D. C. Allan, T. A. Arias, and J. D. Joannopoulos, *Rev. Mod. Phys.* **64**, 1045 (1992).
4. E. G. Moroni, G. Kresse, J. Hafner, and J. Furthmüller, *Phys. Rev.* **B56**, 15629 (1997).
5. N. Chetty, M. Weinert, T. S. Rahman, and J. W. Davenport, *Phys. Rev.* **B52**, 6313 (1995).
6. M. Krajci, J. Hafner, and M. Mihalkovic, *Phys. Rev.* **B56**, 3072 (1997); M. Krajci and J. Hafner, *Phys. Rev.* **B58**, 5378 (1998).
7. C. G. Morgan, P. Kratzer, M. Scheffler, *Phys. Rev. Lett.* **82**, 4886 (1999).

8. R. N. Barnett and U. Landman, *Phys. Rev.* **B48**, 2081 (1993).
9. M. Eichinger, P. Tavan, J. Hutter, and M. Parinello, *J. Chem. Phys.* **110**, 10452 (1999); D. Marx, M. E. Tuckerman, J. Hutter, and M. Parinello, *Nature* **397**, 601 (1999).
10. J. C. Phillips and L. Kleinman, *Phys. Rev.* **116**, 287 (1959); L. Kleinman and J. C. Phillips, *Phys. Rev.* **116**, 880 (1959); *Phys. Rev.* **117**, 460 (1960); *Phys. Rev.* **118**, 1153 (1960).
11. C. Herring, *Phys. Rev.* **57**, 1169 (1940).
12. V. Heine and I. Abarenkov, *Philos. Mag.* **9**, 451 (1964); I. Abarenkov and V. Heine, *Philos. Mag.* **12**, 529 (1965); A. O. E. Animalu and V. Heine, *Philos. Mag.* **12**, 1249 (1965).
13. N. W. Ashcroft, *Phys. Lett.* **23**, 48 (1966); N. W. Ashcroft and D. C. Langreth, *Phys. Rev.* **155**, 682 (1967).
14. C. Fiolhais, J. P. Perdew, S. Q. Armster, J. M. MacLaren, and M. Brajczewska, *Phys. Rev.* **B51**, 14001 (1995); F. Nogueira, C. Fiolhais, and J. P. Perdew, *Phys. Rev.* **B59**, 2570 (1999).
15. D. R. Hamann, M. Schlüter, and C. Chiang, *Phys. Rev. Lett.* **43**, 1494 (1979); G. B. Bachelet, D. R. Hamann, and M. Schlüter, *Phys. Rev.* **B26**, 4199 (1982).
16. G. P. Kerker, *J. Phys.* **C13**, L189 (1980).
17. D. Vanderbilt, *Phys. Rev.* **B32**, 8412 (1985).
18. D. R. Hamann, *Phys. Rev.* **B40**, 2980 (1989).
19. N. Troullier and J. L. Martins, *Phys. Rev.* **B43**, 1993 (1991).
20. S. G. Louie, S. Froyen, and M. L. Cohen, *Phys. Rev.* **B26**, 1738 (1982).
21. T. Sasaki, A. M. Rappe, and S. G. Louie, *Phys. Rev.* **B52**, 12760 (1995).
22. M. Fuchs, M. Bockstedte, E. Pehlke, and M. Scheffler, *Phys. Rev.* **B57**, 2134 (1998).
23. D. Porezag, M. A. Pederson, and A. Y. Liu, *Phys. Rev.* **B60**, 14132 (1999).
24. G. Ortiz and P. Ballone, *Phys. Rev.* **B43**, 6376 (1991).
25. A. D. Becke, *Phys. Rev.* **A38**, 3098 (1988).
26. J. P. Perdew, in *Electronic Structure of Solids 1991*, edited by P. Ziesche and H. Eschrig (Akademie Verlag, Berlin, 1991), p.11; J. P. Perdew, J. A. Chevary, S. H. Vosko, K. A. Jackson, M. R. Pederson, D. J. Singh, and C. Fiolhais, *Phys. Rev.* **B46**, 6671 (1992).
27. D. M. Bylander and L. Kleinman, *Phys. Rev. Lett.* **74**, 3660 (1995); *Phys. Rev.* **B52**, 14566 (1995); *Phys. Rev.* **B54**, 7891 (1996); *Phys. Rev.* **B55**, 9432 (1997).
28. M. Städele, J. A. Majewski, P. Vogl, and A. Görling, *Phys. Rev. Lett.* **79**, 2089 (1997); M. Städele, M. Moukara, J. A. Majewski, P. Vogl, and A. Görling, *Phys. Rev.* **B59**, 10031 (1999). M. Moukara, M. Städele, J. A. Majewski, P. Vogl, and A. Görling, *J. Phys.* **C12**, 6783 (2000).
29. A. Höck and E. Engel, *Phys. Rev.* **A58**, 3578 (1998).
30. Y.-H. Kim, M. Städele, and R. M. Martin, *Phys. Rev.* **B60**, 3633 (1999).
31. V. Sahni, J. Gruenebaum, and J. P. Perdew, *Phys. Rev.* **B26**, 4371 (1982).

32. D. C. Langreth and M. J. Mehl, *Phys. Rev.* **B28**, 1809 (1983).
33. A. Görling and M. Levy, *Phys. Rev.* **A50**, 196 (1994).
34. T. Grabo and E. K. U. Gross, *Chem. Phys. Lett.* **240**, 141 (1995); T. Grabo, T. Kreibich, and E. K. U. Gross, *Mol. Engineering* **7**, 27 (1997).
35. T. Kotani, *J. Phys.: Condens. Matter* **10**, 9241 (1998).
36. E. Engel, A. Facco Bonetti, S. Keller, I. Andrejkovics, and R. M. Dreizler, *Phys. Rev.* **A58**, 964 (1998).
37. E. Engel and A. Facco Bonetti, in: *Quantum Systems in Theoretical Chemistry and Physics, Vol.1: Basic Problems and Model Systems*, ed. by A. Hernández-Laguna, J. Maruani, R. McWeeny, and S. Wilson (Kluwer, Dordrecht, 2000), p.227.
38. M. Seidl, J. P. Perdew, and S. Kurth, *Phys. Rev. Lett.* **84**, 5070 (2000).
39. A. Facco Bonetti, E. Engel, R. N. Schmid, and R. M. Dreizler, *Phys. Rev. Lett.* **86**, 2241 (2001).
40. E. Engel and R. M. Dreizler, *J. Comput. Chem.* **20**, 31 (1999).
41. J. B. Krieger, Y. Li, and G. J. Iafrate, *Phys. Lett.* **A146**, 256 (1990); *Phys. Lett.* **A148**, 470 (1990); Y. Li, J. B. Krieger, M. R. Norman and G. J. Iafrate, *Phys. Rev.* **B44**, 10437 (1991); Y. Li, J. B. Krieger, and G. J. Iafrate, *Chem. Phys. Lett.* **191**, 38 (1992); J. B. Krieger, Y. Li and G. J. Iafrate, *Phys. Rev.* **A45**, 101 (1992); *Phys. Rev.* **A46**, 5453 (1992); Y. Li, J. B. Krieger, and G. J. Iafrate, *Phys. Rev.* **A47**, 165 (1993).
42. E. Engel, J. A. Chevary, L. D. Macdonald, and S. H. Vosko, *Z. Phys.* **D23**, 7 (1992); E. Engel and S. H. Vosko, *Phys. Rev.* **A47**, 2800 (1993); *Phys. Rev.* **B47**, 13 164 (1993); *Phys. Rev.* **B50**, 10498 (1994); E. Engel, S. Keller, A. Facco Bonetti, H. Müller, and R. M. Dreizler, *Phys. Rev.* **A52**, 2750 (1995).
43. T. Kotani, *Phys. Rev.* **B50**, 14816 (1994); *Phys. Rev. Lett.* **74**, 2989 (1995); T. Kotani and H. Akai, *Phys. Rev.* **B54**, 16 502 (1996).
44. S. J. A. van Gisbergen, P. R. T. Schipper, O. V. Gritsenko, E. J. Baerends, J. G. Snijders, B. Champagne, and B. Kirtman, *Phys. Rev. Lett.* **83**, 694 (1999).
45. S. Ivanov, S. Hirata, and R. J. Bartlett, *Phys. Rev. Lett.* **83**, 5455 (1999).
46. A. Görling, *Phys. Rev. Lett.* **83**, 5459 (1999).
47. E. Engel, A. Höck and R. M. Dreizler, *Phys. Rev.* **A61**, 032502 (2000).
48. E. Engel, A. Höck and R. M. Dreizler, *Phys. Rev.* **A62**, 042502 (2000).
49. R. T. Sharp and G. K. Horton, *Phys. Rev.* **90**, 317 (1953).
50. J. D. Talman and W. F. Shadwick, *Phys. Rev.* **A14**, 36 (1976).
51. A. Bergner, M. Dolg, W. Küchle, H. Stoll, and H. Preuß, *Mol. Phys.* **80**, 1431 (1993).
52. E. Engel, A. Höck, and S. Varga, *Phys. Rev.* **B63**, 125121 (2001).
53. E. Engel, A. Höck, R. N. Schmid, R. M. Dreizler, and N. Chetty, to be published.
54. M. E. Rose, *Elementary Theory of Angular Momentum* (Wiley, New York, 1957).
55. Note that, in principle, this problem is also relevant for explicitly density-

dependent functionals, as the derivation of the KS equations relies on the multiplicative nature of the total single-particle potential.

56. For the LDA correlation functional the parametrization of S. H. Vosko, L. Wilk, and M. Nusair, *Can. J. Phys.* **58**, 1200 (1980), has been used.
57. H. A. Fertig and W. Kohn, *Phys. Rev.* **A62**, 052511 (2000).
58. F. W. Kutzler and G. S. Painter, *Phys. Rev. Lett.* **59**, 1285 (1987).
59. For  $v_{loc}$  we have always used the  $p$ -PP in the case of the first row elements and the  $d$ -PP for the second row atoms.
60. C. Filippi, D. J. Singh, and C. J. Umrigar, *Phys. Rev.* **B50**, 14947 (1994); A. Khein, D. J. Singh, and C. J. Umrigar, *Phys. Rev.* **B51**, 4105 (1995).
61. K. P. Huber and G. L. Herzberg, *Molecular Spectra and Molecular Structure. IV. Constants of Diatomic Molecules* (Van Nostrand Reinhold, New York, 1979).
62. H. J. Monkhorst and J. D. Pack, *Phys. Rev.* **B13**, 5188 (1976).